# Intelligent backstepping sliding-mode control using RBFN for two-axis motion control system

P.-H. Shen and F.-J. Lin

**Abstract:** An intelligent backstepping sliding-mode control system using radial basis function network (RBFN) for a two-axis motion control system using permanent magnet linear synchronous motors (PMLSMs) is proposed. First, single-axis motion dynamics with the introduction of a lumped uncertainty, including cross-coupled interference between the two-axis mechanism, is derived. Then, to improve the control performance in reference contour tracking, a backstepping sliding-mode approach is proposed to compensate for uncertainties occurring in the motion control system. The bound of the lumped uncertainty is necessary in the design of the backstepping sliding-mode control system and is difficult to obtain in advance in practical applications. Therefore, an RBFN uncertainty observer is proposed to estimate the required lumped uncertainty in the backstepping sliding-mode control system. An adaptive learning algorithm, which can learn the parameters of the RBFN online, is derived using Lyapunov stability theorem. The proposed control algorithms are implemented in a TMS320C32 DSP-based control computer, and the motions in the $x$-axis and $y$-axis are controlled separately. The simulated and experimental results of circle and four leaves reference contours show that the motion tracking performance is significantly improved and the robustness to parameter variations, external disturbances, cross-coupled interference and frictional forces can also be obtained using the proposed controller.

## 1 Introduction

In modern manufacturing systems, computer numerical controlled (CNC) machines have become important elements [1–3]. CNC machines generally can be divided into two types: mechanical types with servo drive systems and servo controllers that control the multi-axis motion of the mechanical parts. In general, the CNC machine consists of an $x$–$y$ table and a $z$-axis motion mechanism, where each motion axis is driven by an individual actuator system, such as DC or AC motors. The motion mechanisms using motor drives usually lead to the existence of the unmodelled dynamics, coupled interferences, unmeasured friction, and disturbances between each other, which often deteriorate the system performance significantly in machining processes [1]. Therefore, in order to improve the tracking performance in machining processes, many studies have been presented [4–6]. In addition, the design of two-axis motion control with high-performance and high-precision machining is required in modern manufacturing. Since the direct drive design of mechanical applications based on PMLSM is a viable candidate to meet the increasing demands for higher contouring accuracy at high machine speeds [7–11], the motion control of an $x$–$y$ table consisting of two PMLSMs is considered in this paper. The direct drive design based on PMLSM has the following advantages over its indirect counterpart: no backlash and less friction; high speed and high precision in long-distance locations; simple mechanical construction, resulting in higher reliability and frame stiffness; and high thrust force [7]. However, the servo performance of the PMLSM is greatly affected by uncertainties, including parameter variations, external disturbances and unmodelled dynamics in the drive system since it is not equipped with auxiliary mechanisms such as gears or ball screws. Furthermore, since the operation of PMLSM involves two contacting bodies, a nonlinear friction force is inevitably among the forces of motion. The friction characteristic may easily be varied owing to the change of normal forces in contact, temperature and humidity [12, 13]. Besides, in a closed-loop control system, the nonlinear friction force often results in steady-state error, limit cycle and low bandwidth [12, 13].

Adaptive backstepping is a systematic and recursive design methodology for nonlinear feedback control [14–18]. In many cases, the feedback linearisation method using geometric approach [19] is only valid in some local region and with a disturbance-free setting. The adaptive backstepping design alleviates some of these limitations [14–16]. Moreover, while the feedback linearisation method requires precise modelling and often cancels some useful nonlinearities [19], the adaptive backstepping design offers a choice of design tools for accommodation of uncertainties and nonlinearities and can avoid wasteful cancellations. Furthermore, the adaptive backstepping control approach is capable of keeping almost all the robustness properties [14–18]. The idea of backstepping design is to select recursively some appropriate functions of state variables as pseudo-control inputs for lower dimension subsystems of the overall system. Each backstepping stage results in a new pseudo-control design, expressed in terms of the pseudo-control designs from preceding design stages. When the procedure terminates, a feedback design for the true control



*IEE Proceedings* online no. 20050103

doi:10.1049/ip-epa:20050103

Paper first received 28th March and in final revised form 9th June 2005

The authors are with the Department of Electrical Engineering, National Dong Hwa University, Hualien 974, Taiwan, Republic of China

E-mail: linfj@mail.ndhu.edu.tw

input results, which achieves the original design objective by virtue of a final Lyapunov function formed by summing up the Lyapunov functions associated with each individual design stage [16]. In addition, owing to the robust control performance of adaptive backstepping control and sliding-mode control, numerous combined adaptive backstepping and sliding-mode control schemes have appeared for both linear and nonlinear systems [20–23].

Intelligent control approaches, such as neural networks and fuzzy systems, do not require mathematical models and have the ability to approximate nonlinear systems. Therefore, many researchers used intelligent control approaches to represent complex plants and construct advanced controllers [24]. Moreover, the locally tuned and overlapped receptive field is a well-known structure that has been studied in regions of the cerebral cortex, visual cortex, and so on [24]. Based on the biological receptive fields, the RBFN, which employs local receptive fields to perform function mappings, was proposed in [25]. Furthermore, the RBFN has a faster convergence property than a multilayer perceptron (MLP) because the RBFN has a simple structure. In addition, the RBFN has a similar feature to the fuzzy system. First, the output value is calculated using the weighted sum method. Then, the number of nodes in the hidden layer of the RBFN is the same as the number of if–then rules in the fuzzy system. Finally, the receptive field functions of the RBFN are similar to the membership functions of the premise part in the fuzzy system. Therefore, the RBFN is very useful for application in controlling dynamic systems [26, 27].

In this paper, an intelligent backstepping sliding-mode control system using RBFN is designed to control the position of mover of an $x$–$y$ table using two PMLSMs. First, in order to obtain the simplified control design, the single-axis dynamics of the field-oriented control PMLSM with the introduction of a lumped uncertainty, which includes parameter variations, external disturbances, cross-coupled interference and friction force, is derived. The considered lumped uncertainty includes variation of mover mass and unknown external disturbance force, which are the major concerns in motion control applications. Then, a backstepping sliding-mode controller is designed to improve the control performance in reference contour tracking. To increase further the robustness of the $x$–$y$ table machine to uncertainties, an RBFN uncertainty observer is proposed to estimate the required lumped uncertainty in the backstepping sliding-mode control system. Then an online parameter training methodology, which is derived using the Lyapunov stability theorem, is proposed to increase the learning capability of the RBFN. Under the proposed control scheme, the single-axis dynamics of the field-oriented control PMLSM and the robust control performance are obtained by the proposed intelligent backstepping sliding-mode control system using RBFN. In addition, the proposed intelligent control system and the field-oriented mechanism are implemented in a control computer that is based on a 32-bit floating-point DSP, TMS320C32. Additionally, some simulated and experimental results are provided to demonstrate the effectiveness of the proposed control scheme. Finally, the performance measures of the experimental results of the backstepping sliding-mode controller are also discussed for comparison of the control performance.

## 2 Modelling of $x-y$ table machine

The $x$–$y$ table machine used in this study consists of two PMLSMs. The adopted PMLSM includes a long stationary tubular 'secondary' with guidance rail and linear scale, and a moving short 'primary', which contains the core armature winding and Hall sensing elements. The adopted PMLSMs are 220 V 5.0 A 475 N type. The machine model of a single-axis PMLSM can be described in synchronous rotating reference frame as follows [7]:

$$v_{qi} = R_{si} i_{qi} + \dot{\lambda}_{qi} + \omega_{ei} \lambda_{di} \tag{1}$$

$$v_{di} = R_{si} i_{di} + \dot{\lambda}_{di} - \omega_{ei} \lambda_{qi} \tag{2}$$

where

$$\lambda_{qi} = L_{qi} i_{qi} \tag{3}$$

$$\lambda_{di} = L_{di} i_{di} + \lambda_{PMi} \tag{4}$$

$$\omega_{ei} = n_{pi} \omega_{ri} \tag{5}$$

and $i = x, y$ ($x$ and $y$ denote the axis); $v_{di}$, $v_{qi}$ are the $d$–$q$ axis voltages; $i_{di}$, $i_{qi}$ are the $d$–$q$ axis currents; $R_{si}$ is the phase winding resistance; $L_{di}$, $L_{qi}$ are the $d$–$q$ axis inductances; $\omega_{ri}$ is the angular velocity of the mover; $\omega_{ei}$ is the electrical angular velocity; $\lambda_{PMi}$ is the permanent magnet flux linkage; and $n_{pi}$, which is 1, is the number of primary pole pairs. Also,

$$\omega_{ri} = \pi v_i / \tau_i \tag{6}$$

$$v_{ei} = n_{pi} v_i = 2\tau_i f_{ei} \tag{7}$$

where $v_i$ is the linear velocity of the mover; $\tau_i$, which is 32 mm, is the pole pitch; $v_{ei}$ is the electric linear velocity; $f_{ei}$ is the electric frequency. The developed electromagnetic power is given by

$$P_{ei} = F_{ei} v_{ei} = 3 n_{pi} [\lambda_{di} i_{qi} + (L_{di} - L_{qi}) i_{di} i_{qi}] \omega_{ei} / 2 \tag{8}$$

Thus, the electromagnetic force is

$$F_{ei} = 3\pi n_{pi} [\lambda_{di} i_{qi} + (L_{di} - L_{qi}) i_{di} i_{qi}] / 2\tau_i \tag{9}$$

The configuration of a single-axis field-oriented control PMLSM servo drive system is shown in Fig. 1 [11], where $d_{mi}$ is the position command; $d_i$ is the position of the motor; $v_{mi}$ is the velocity command; $v_i$ is the linear velocity of the mover; $i^*_{ai}$, $i^*_{bi}$ and $i^*_{ci}$ are the three-phase command currents; $i_{ai}$ and $i_{bi}$ are the $A$ and $B$ phase currents; $T_{ai}$, $T_{bi}$ and $T_{ci}$ are the switching signals of the inverter; and $i^*_{di}$ is the flux current command. The drive system consists of a PMLSM, a ramp comparison current-controlled PWM VSI, a field-orientation mechanism, a co-ordinate translator, a speed control loop, a position control loop, a linear scale and Hall sensors. The flux position of the PM ($\theta_{ei}$) is detected by the output signals of the Hall sensors ($U_i$, $V_i$, $W_i$) and the mover position signal $d_i$. Different sizes of iron discs can be mounted on the mover of the PMLSM to change the mass of the moving element. With the implementation of the field-oriented control, the electromagnetic force can be simplified as follows:

$$F_{ei} = K_{fi} i^*_{qi} \tag{10}$$

$$K_{fi} = 3\pi n_{pi} \lambda_{PMi} / (2\tau_i) \tag{11}$$

where $K_{fi}$ is the thrust coefficient and $i^*_{qi}$ is the thrust current command. The mover dynamic equation using the electromagnetic force shown in (10) is

$$F_{ei} = M_i \dot{v}_i + D_i v_i + F_{Li} + f_i(v) \tag{12}$$

where $M_i$ is the total mass of the mover; $D_i$ is the viscous friction and iron-loss coefficient; $F_{Li}$ includes the external disturbances and the cross-coupled interference due to two-axis mechanism; and $f_i(v)$ is the friction force. Considering

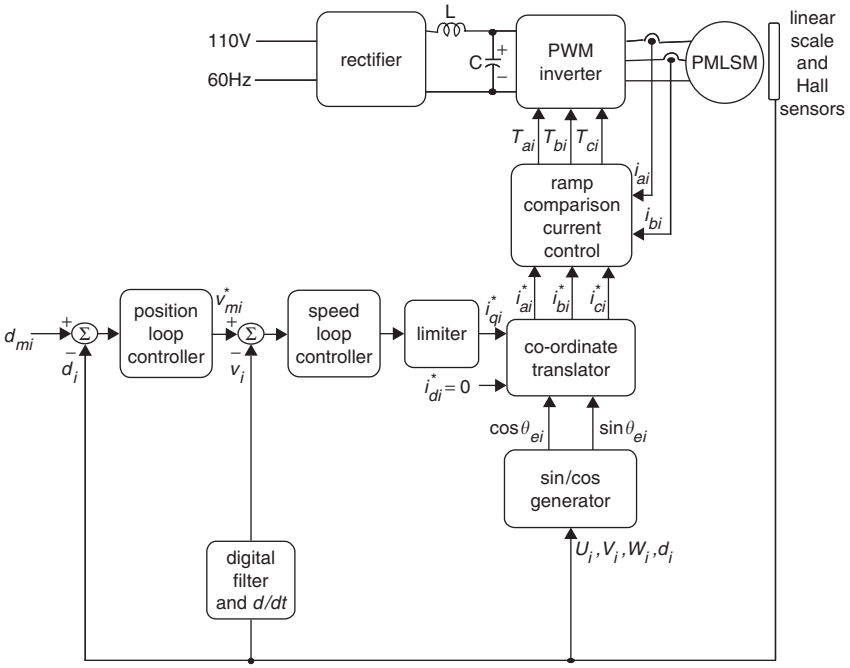


**Fig. 1** *System configuration of field-oriented control PMLSM servo drive*

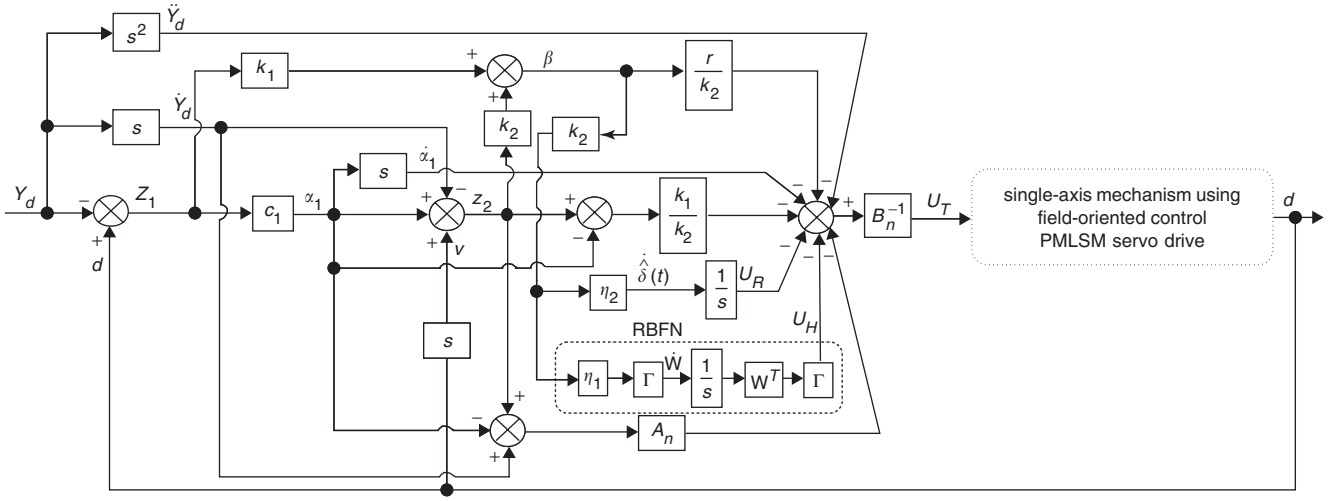


**Fig. 2** *Intelligent backstepping sliding-mode control system using RBFN*

Coulomb friction, viscous friction and the Stribeck effect, the friction force can be formulated as follows [12, 13]:

$$f_i(v) = F_{Ci}\,\mathrm{sgn}(v_i) + (F_{Si} - F_{Ci})e^{-(v_i/v_{si})^2}\mathrm{sgn}(v_i) + K_{vi}v_i \tag{13}$$

where $F_{Ci}$ is the Coulomb friction; $F_{Si}$ is the static friction; $v_{Si}$ is the Stribeck velocity parameter; $K_{vi}$ is the coefficient of viscous friction; and sgn$(\cdot)$ is a sign function. All the parameters in (13) are time-varying.

Curve-fitting techniques based on step response of the mover position are applied here to find the model of the drive system. For the convenience of the controller design, the position and speed signals in the control loop are set at $1\,\mathrm{V} = 0.063662\,\mathrm{m}$ and $1\,\mathrm{V} = 0.063662\,\mathrm{m/s}$. The major system parameters are

$$\begin{aligned} &\bar{K}_{fx} = 95\,\mathrm{N/A},\ \bar{M}_x = 6.32\,\mathrm{kg} = 0.4023\,\mathrm{Ns/V},\\ &\bar{D}_x = 819.4069\,\mathrm{kg/s} = 52.1651\,\mathrm{N/V} \end{aligned} \tag{14}$$

$$\begin{aligned} &\bar{K}_{fy} = 95\,\mathrm{N/A},\ \bar{M}_y = 17.65\,\mathrm{kg} = 1.1236\,\mathrm{Ns/V},\\ &\bar{D}_y = 1716.2789\,\mathrm{kg/s} = 109.2617\,\mathrm{N/V} \end{aligned} \tag{15}$$

The overbar symbol represents the system parameter in the nominal condition. Although the electromagnetic force can be simplified as (10) via the field-oriented control, considering the variations of system parameters and external disturbances, including cross-coupled interference and friction force, the $x$–$y$ table machine is a nonlinear time-varying system in practical applications.

## 3 Intelligent backstepping sliding-mode control system using RBFN

To control the motion of an $x$–$y$ table, an intelligent backstepping sliding-mode control system using RBFN is proposed. The motions of the $x$-axis and $y$-axis are controlled separately. The configuration of the proposed intelligent backstepping sliding-mode control system using RBFN for a single-axis PMLSM is shown in Fig. 2. All the

subscripts $i$ are removed for simplicity in the descriptions of this Section, including those in Fig. 2.

Each field-oriented control PMLSM servo drive can be formulated by rewriting (10) and (12) as follows:

$$\ddot{d}(t) = -\frac{D}{M}\dot{d}(t) + \frac{K_f}{M}i_q^*(t) - \frac{1}{M}[F_L + f(v)] \underline{\underline{\Delta}} A_p\dot{d}(t) + B_pU_T + C_p[F_L + f(v)] \quad (16)$$

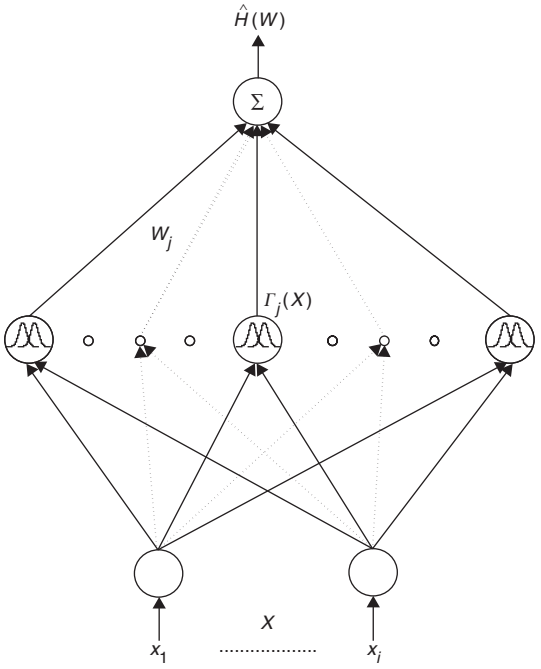


**Fig. 3** *Structure of RBFN*

where $A_p = -D/M$; $B_p = K_f/M > 0$; $C_p = -1/M$; and $U_T$ is the control effort, i.e. the thrust current command. Now, considering the existence of parameter variations and external force disturbances including cross-coupled interference and friction force for the single-axis field-oriented control PMLSM servo drive system,

$$\dot{X}_U = X_P \quad (17)$$

$$\dot{X}_P = (A_n + \Delta A)X_p + (B_n + \Delta B)U_T + C_p[F_L + f(v)] \quad (18)$$

$$Y = X_U \quad (19)$$

where $X_U = d(t)$; $X_P = v(t)$; $A_n$ is the nominal value of $A_p$; $B_n$ is the nominal value of $B_p$; and $\Delta A$ and $\Delta B$ denote the uncertainties introduced by system parameters $M$ and $D$. Reformulate (18) as

$$\dot{X}_P = A_nX_P + B_nU_T + H \quad (20)$$

where $H$ is named the lumped uncertainty and defined by

$$H \equiv \Delta AX_P + \Delta BU_T + C_p[F_L + f(v)] \quad (21)$$

The lumped uncertainty $H$ will be observed by an RBFN and assumed to be a constant during the observation. The above assumption is valid in practical digital processing of the observer since the sampling period of the observer is short enough compared with the variation of $H$.

The control objective is to design an intelligent backstepping sliding-mode control system for the output $Y$ of the system shown in (19) to track the desired command $Y_d(t)$, which is $d_m(t)$, asymptotically. Assume that not only $Y_d(t)$ but also its first two derivatives $\dot{Y}_d(t)$ and $\ddot{Y}_d(t)$ are all

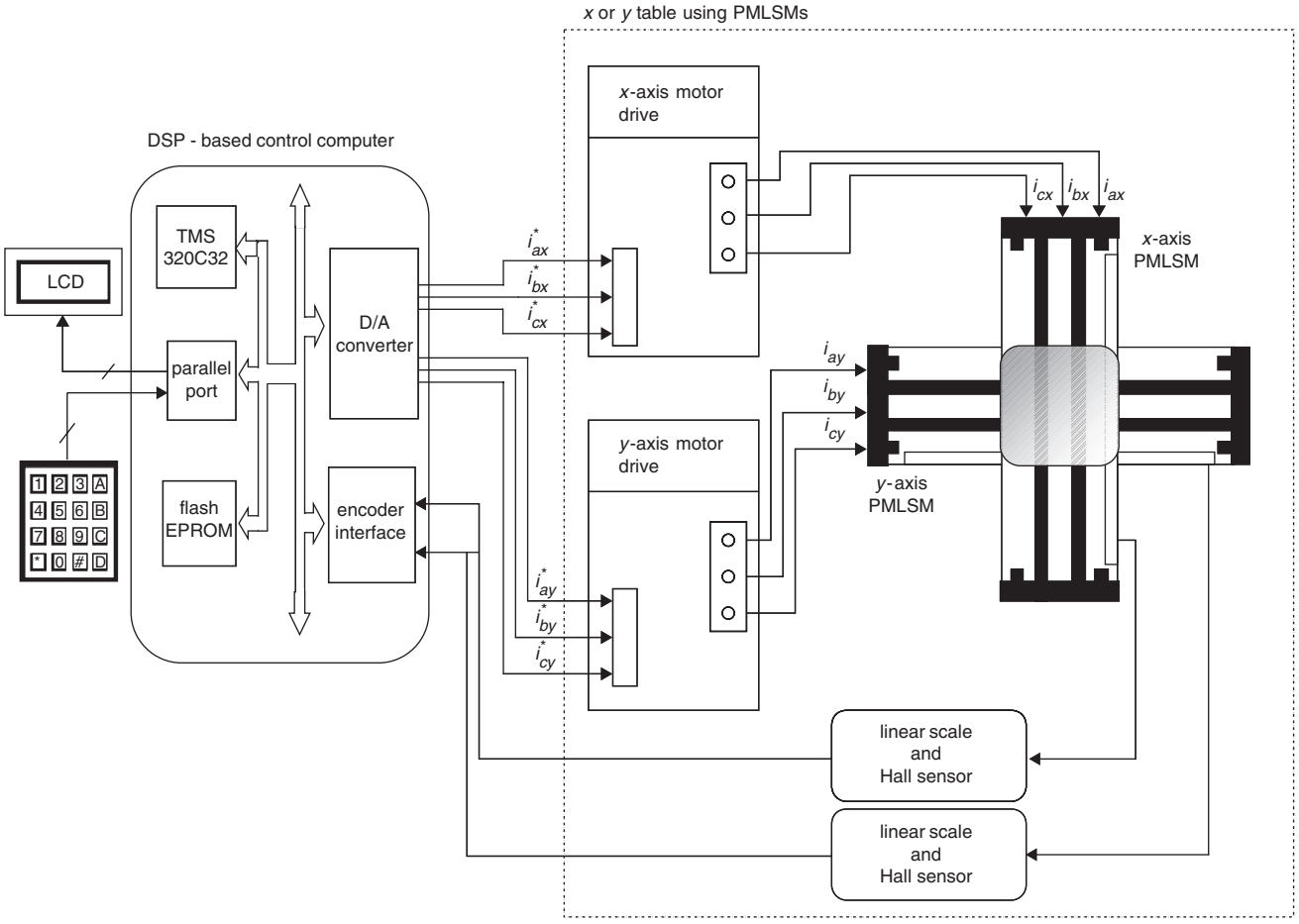


**Fig. 4** *DSP-based two-axis motion control system*

bounded functions of time. The proposed intelligent backstepping sliding-mode control system using RBFN is designed to achieve the position-tracking objective and is described step-by-step as follows:

### 3.1 Step 1

For the position-tracking objective, define the tracking error as

$$z_1 = Y - Y_d \tag{22}$$

and its derivative is

$$\dot{z}_1 = X_P - \dot{Y}_d \tag{23}$$

Define the following stabilising function:

$$\alpha_1 = c_1 z_1 \tag{24}$$

where $c_1$ is a positive constant. The first Lyapunov function is chosen as

$$V_1 = z_1^2/2 \tag{25}$$

Define $z_2 = X_P - \dot{Y}_d + \alpha_1$, then the derivative of $V_1$ is

$$\dot{V}_1 = z_1(X_p - \dot{Y}_d) = z_1(z_2 - \alpha_1) = z_1 z_2 - c_1 z_1^2 \tag{26}$$

### 3.2 Step 2

The derivative of $z_2$ is now expressed as

$$\dot{z}_2 = \dot{X}_P - \ddot{Y}_d + \dot{\alpha}_1 = A_n X_p + B_n U_T + H - \ddot{Y}_d + \dot{\alpha}_1 \tag{27}$$

To design the backstepping sliding-mode control system, the lumped uncertainty is assumed to be bounded, i.e. $|H| \le \rho$, and the following Lyapunov function is defined:

$$V_2 = V_1 + \frac{1}{2}\beta^2 \tag{28}$$

with the sliding surface

$$\beta = k_1 z_1 + k_1 z_2 \tag{29}$$

Using (26) and (27), the derivative of $V_2$ can be derived as follows:

$$\begin{aligned}\dot{V}_2 &= \dot{V}_1 + \beta\dot{\beta} = z_1 z_2 - c_1 z_1^2 + \beta\dot{\beta} \\ &= z_1 z_2 - c_1 z_1^2 + \beta(k_1 \dot{z}_1 + k_2 \dot{z}_2) \\ &= z_1 z_2 - c_1 z_1^2 + \beta\{k_1(z_2 - \alpha_1) \\ &\quad + k_2[A_n(z_2 + \dot{Y}_d - \alpha_1) \\ &\quad + B_n U_T + H - \ddot{Y}_d + \dot{\alpha}_1]\}\end{aligned} \tag{30}$$

According to (30), a backstepping sliding-mode control law $U_T$ is designed as follows:

$$\begin{aligned}U_T = B_n^{-1}\Bigg[&-\frac{k_1}{k_2}(z_2 - \alpha_1) - A_n(z_2 + \dot{Y}_d - \alpha_1) \\ &-U_H + \ddot{Y}_d - \dot{\alpha}_1 - \frac{r}{k_2}\beta\Bigg]\end{aligned} \tag{31}$$

where $k_1$, $k_2$ and $r$ are positive constants; and $U_H$ is a robust controller, which is designed to confront the lumped uncertainty as follows:

$$U_H = \rho \mathrm{sgn}(\beta) \tag{32}$$

Substituting (31) and (32) into (30), the following equation can be obtained:

$$\begin{aligned}\dot{V}_2 &= -c_1 z_1^2 + z_1 z_2 - r\beta^2 + k_2[H\beta - \rho|\beta|] \\ &\le -c_1 z_1^2 + z_1 z_2 - r\beta^2 + k_2|\beta|(|H| - \rho) \\ &\le -c_1 z_1^2 + z_1 z_2 - r\beta^2\end{aligned} \tag{33}$$

Note that (33) can be rewritten

$$\dot{V}_2 = -\boldsymbol{z}^T \boldsymbol{P} \boldsymbol{z} \le 0 \tag{34}$$

where $\boldsymbol{P}$ is a positive definite symmetric matrix with the following form

$$\boldsymbol{P} = \begin{bmatrix} c_1 + rk_1^2 & rk_1 k_2 - 1/2 \\ rk_1 k_2 - 1/2 & rk_2^2 \end{bmatrix} \tag{35}$$

and $\boldsymbol{z}^T = [z_1 \quad z_2]$. Note that the determinants of the principal minors of $\boldsymbol{P}$ are all positive; a sufficient condition to guarantee that $\boldsymbol{P}$ is positive definite is

$$\begin{aligned}|\boldsymbol{P}| &= rk_2^2(c_1 + rk_1^2) - \left(\frac{1}{2} - rk_1 k_2\right)^2 \\ &= rk_2(c_1 k_2 + k_1) - \frac{1}{4} > 0\end{aligned} \tag{36}$$

Define the following term:

$$\Omega(t) = \mathbf{z}^T \boldsymbol{P} \mathbf{z} \le -\dot{V}_2(z_1(t), z_2(t)) \tag{37}$$

Then

$$\int_0^t \Omega(\tau)\, d\tau \le V_2(z_1(0), z_2(0)) - V_2(z_1(t), z_2(t)) \tag{38}$$

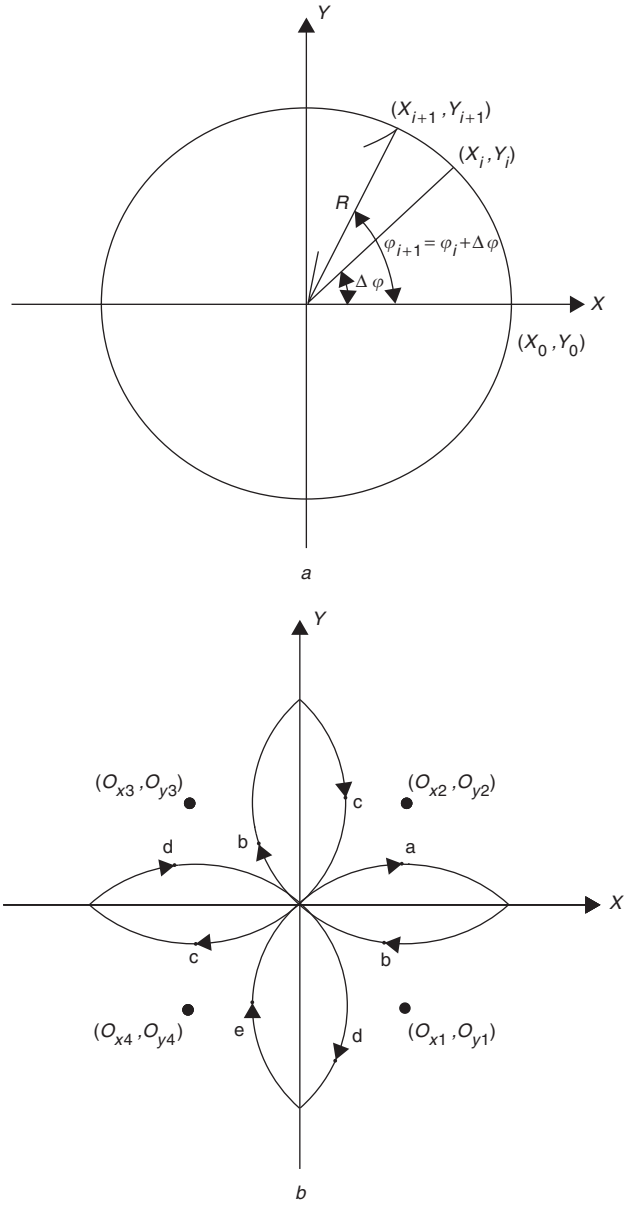


**Fig. 5** *Reference contours*
*a* Circle contour
*b* Four leaves contour

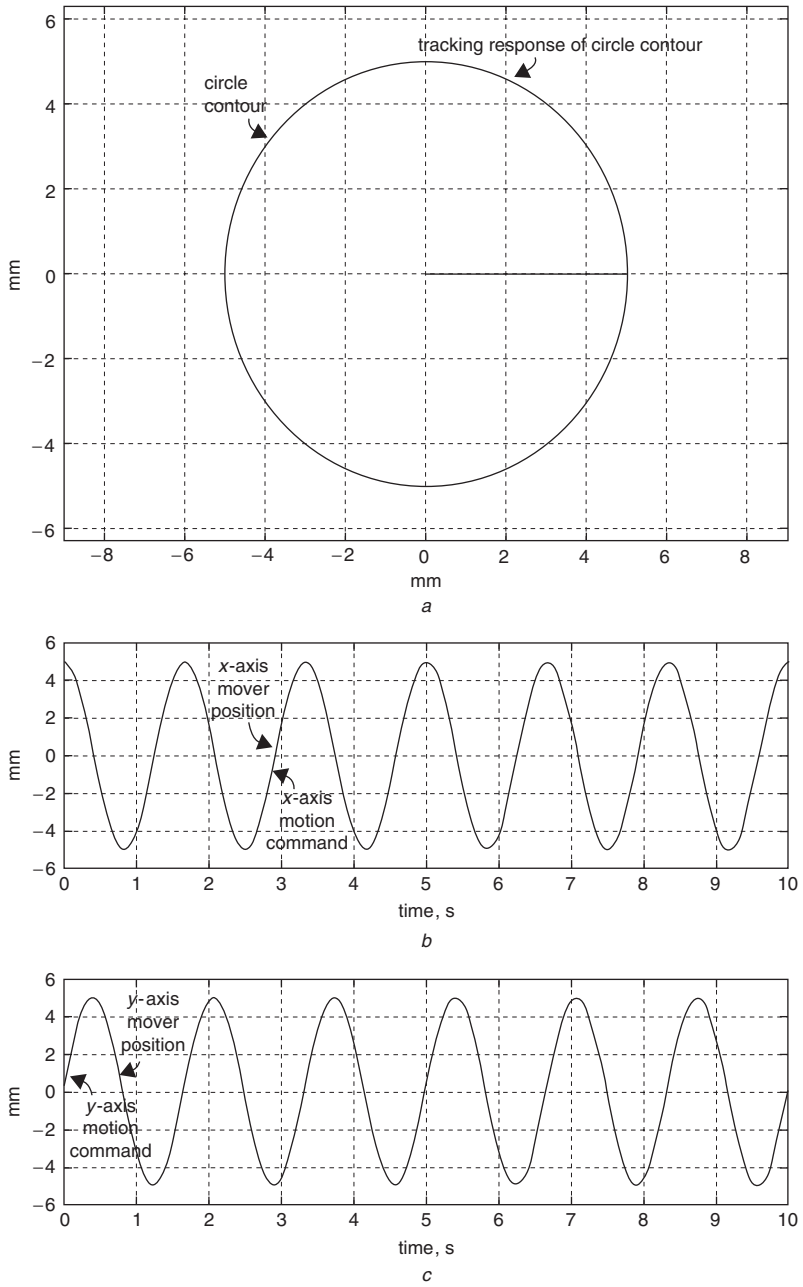


**Fig. 6** *Simulated responses of intelligent backstepping sliding-mode control system due to circle contour for Case 1*
*a* Tracking response of *x*–*y* table
*b* Tracking response of *x*-axis
*c* Tracking response of *y*-axis
*d* Control effort of *x*-axis
*e* Control effort of *y*-axis
*f* Tracking error of *x*-axis
*g* Tracking error of *y*-axis

Since $V_2(z_1(0), z_2(0))$ is bounded and $V_2(z_1(t), z_2(t))$ is nonincreasing and bounded, the following result can be concluded:

$$\lim_{t\to\infty} \int_0^t \Omega(\tau)d\tau < \infty \tag{39}$$

Moreover, $\dot{\Omega}(t)$ is also bounded. Then, $\Omega(t)$ is uniformly continuous. Using Barbalat's lemma [19], the following result can be obtained:

$$\lim_{t\to\infty} \Omega(t) = 0 \tag{40}$$

That is $z_1$ and $z_2$ will converge to zero as $t \to \infty$. Moreover, $\lim_{t\to\infty} Y(t) = Y_d$ and $\lim_{t\to\infty} X_p(t) = \dot{Y}_d$. Therefore, the backstepping sliding-mode control system is asymptotically stable even if parametric uncertainty, external force disturbance, cross-coupled interference and friction force exist.

### 3.3 Step 3

Since the lumped uncertainty $H$ is unknown in practical application, the upper bound $\rho$ is difficult to determine; therefore an RBFN uncertainty observer is proposed to adapt the value of the lumped uncertainty $\hat{H}$. The architecture of an RBFN with $N$ receptive field units is shown in Fig. 3 and the receptive field function is usually a Gaussian function or a logistic function [25]. If the Gaussian function is selected as the receptive field function and assuming that the input vector of the RBFN is $\boldsymbol{X} = [x_1\, x_2\, \cdots\, x_i]^T$ and

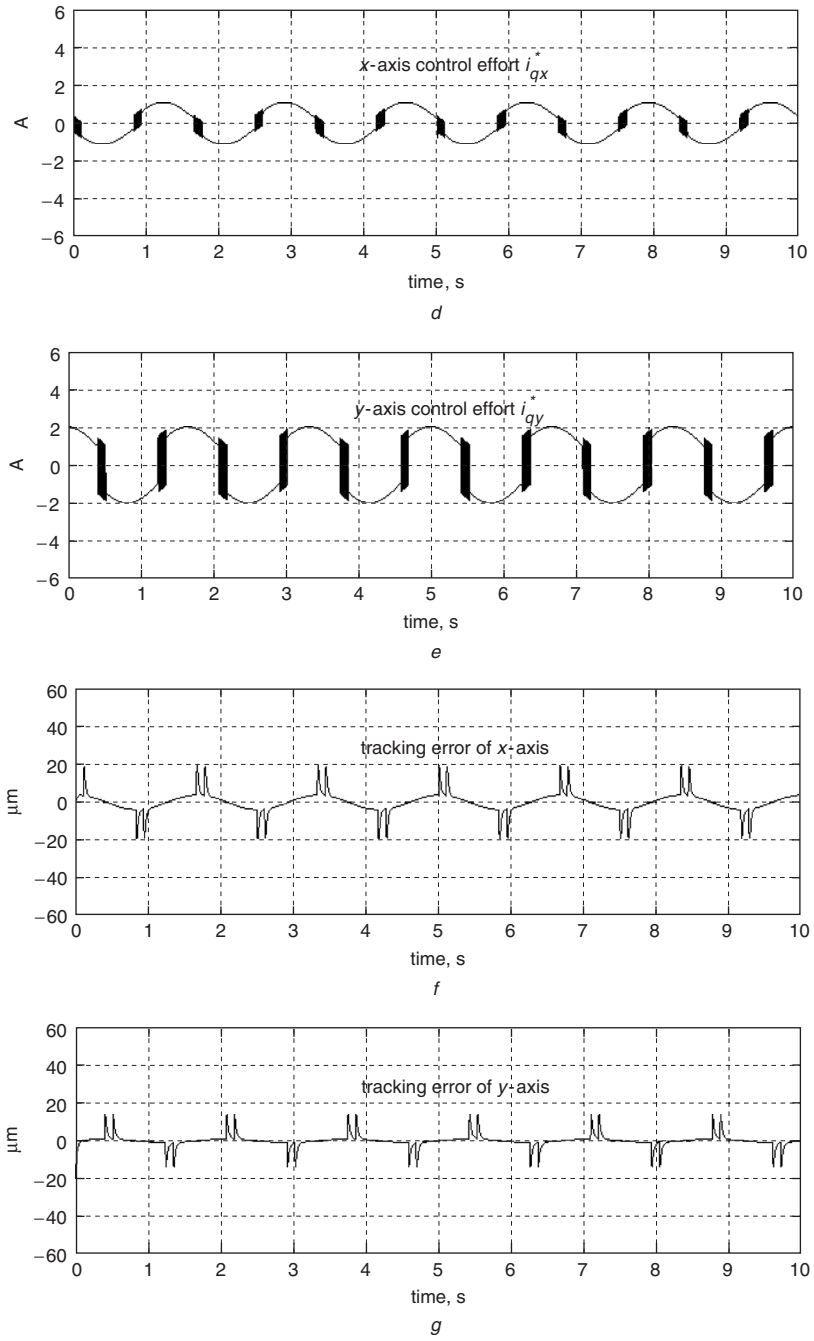


**Fig. 6** *Continued*

using the weighted sum method to calculate the output of the RBFN, then the output becomes

$$\hat{H} = \sum_{j=1}^{N} W_j \Gamma_j(\boldsymbol{X}) \tag{41}$$

$$\Gamma_j(\boldsymbol{X}) = \exp[-(\boldsymbol{X} - \boldsymbol{M}_j)^T \sum_j (\boldsymbol{X} - \boldsymbol{M}_j)],$$

$$j = 1, 2, \ldots, N \tag{42}$$

where $W_j$ is the connective weight between the hidden layer and the output layer, the mean vector $\boldsymbol{M}_j = [m_{1j}\, m_{2j} \cdots m_{ij}]^T$ and the standard deviation vector $\sum_j = \text{diag}[1/s_{1j}^2\ 1/s_{2j}^2 \cdots 1/s_{ij}^2]^T$. The inputs of the RBFN are the tracking error and its derivative, and the output of the RBFN is $\hat{H}$. For ease of discussion, the output of the RBFN is rewritten as:

$$\hat{H}(\boldsymbol{W}) = \boldsymbol{W}^T \boldsymbol{\Gamma} \tag{43}$$

where $\boldsymbol{W} = [W_1\, W_2 \cdots W_N]^T$ and $\boldsymbol{\Gamma} = [\Gamma_1\, \Gamma_2 \cdots \Gamma_N]^T$ which are the collected vectors of $W_j$ and $\Gamma_j$, respectively.

To develop the adaptation laws of the RBFN uncertainty observer, the minimum reconstructed error $\delta$ is defined as:

$$\delta = H - \hat{H}(\boldsymbol{W}^*) \tag{44}$$

where $\boldsymbol{W}^*$ is an optimal weight vector that achieves the minimum reconstructed error. Then, a Lyapunov candidate

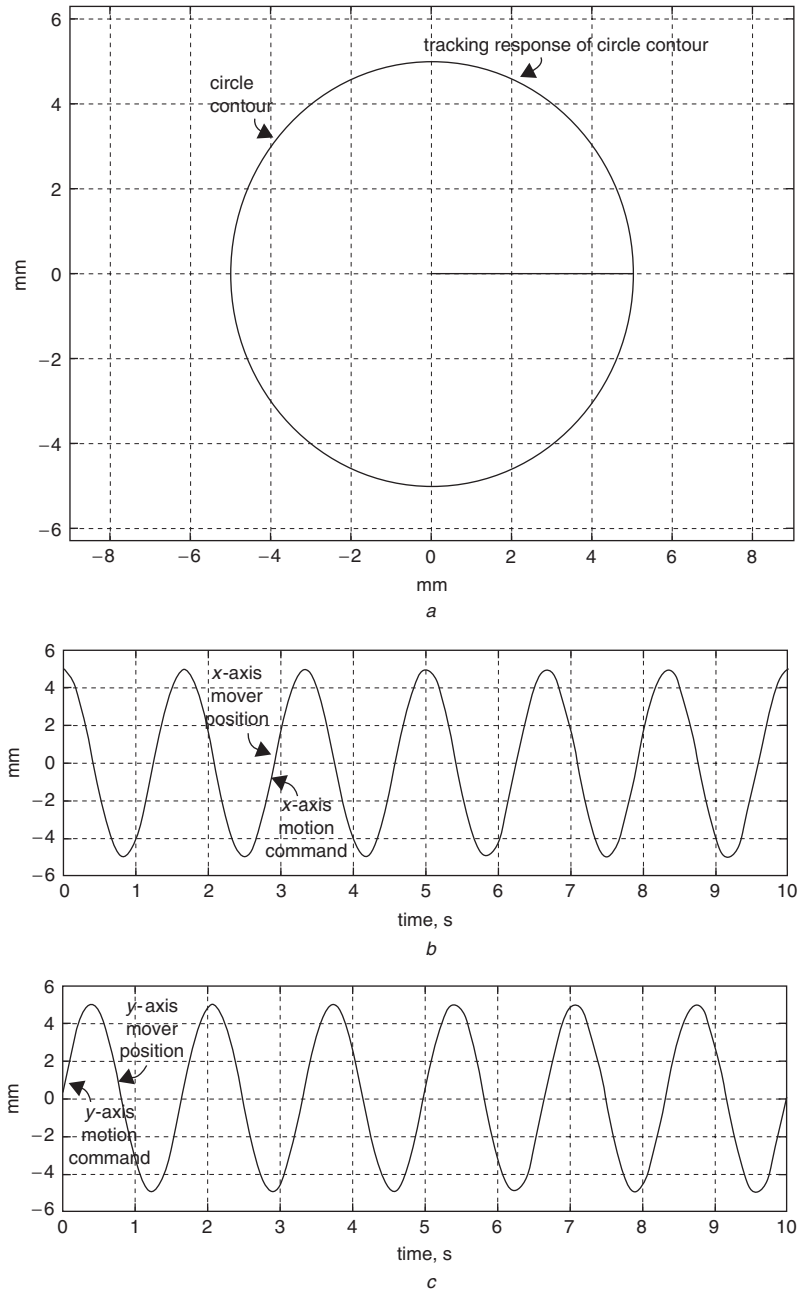


**Fig. 7** *Simulated responses of intelligent backstepping sliding-mode control system due to circle contour for Case 2*
*a* Tracking response of *x–y* table
*b* Tracking response of *x*-axis
*c* Tracking response of *y*-axis
*d* Control effort of *x*-axis
*e* Control effort of *y*-axis
*f* Tracking error of *x*-axis
*g* Tracking error of *y*-axis

is chosen as

$$V_3 = V_2 + \frac{1}{2\eta_1}(\boldsymbol{W}^* - \boldsymbol{W})^T(\boldsymbol{W}^* - \boldsymbol{W}) + \frac{1}{2\eta_2}(\delta - \hat{\delta})^2 \tag{45}$$

where $\eta_1$ and $\eta_2$ are positive constants; and $\hat{\delta}$ is the estimated value of the minimum reconstructed error $\delta$. The estimation of the reconstructed error $\hat{\delta}$ is to compensate for the observed error induced by the RBFN uncertainty observer and to further guarantee the stable characteristic of the whole control system.

Taking the derivative of the Lyapunov function and use (30), then

$$\begin{aligned}\dot{V}_3 &= \dot{V}_2 - \frac{1}{\eta_1}(\boldsymbol{W}^* - \boldsymbol{W})^T\dot{\boldsymbol{W}} - \frac{1}{\eta_2}(\delta - \hat{\delta})\dot{\hat{\delta}} \\ &= z_1 z_2 - c_1 z_1^2 + \beta\{k_1(z_2 - c_1 z_1) + k_2[A_n(z_2 + \dot{Y}_d - \alpha_1) \\ &\quad + B_n U_T + H - \ddot{Y}_d + \dot{\alpha}_1]\} - \frac{1}{\eta_1}(\boldsymbol{W}^* - \boldsymbol{W})^T\dot{\boldsymbol{W}} \\ &\quad - \frac{1}{\eta_2}(\delta - \hat{\delta})\dot{\hat{\delta}}\end{aligned} \tag{46}$$

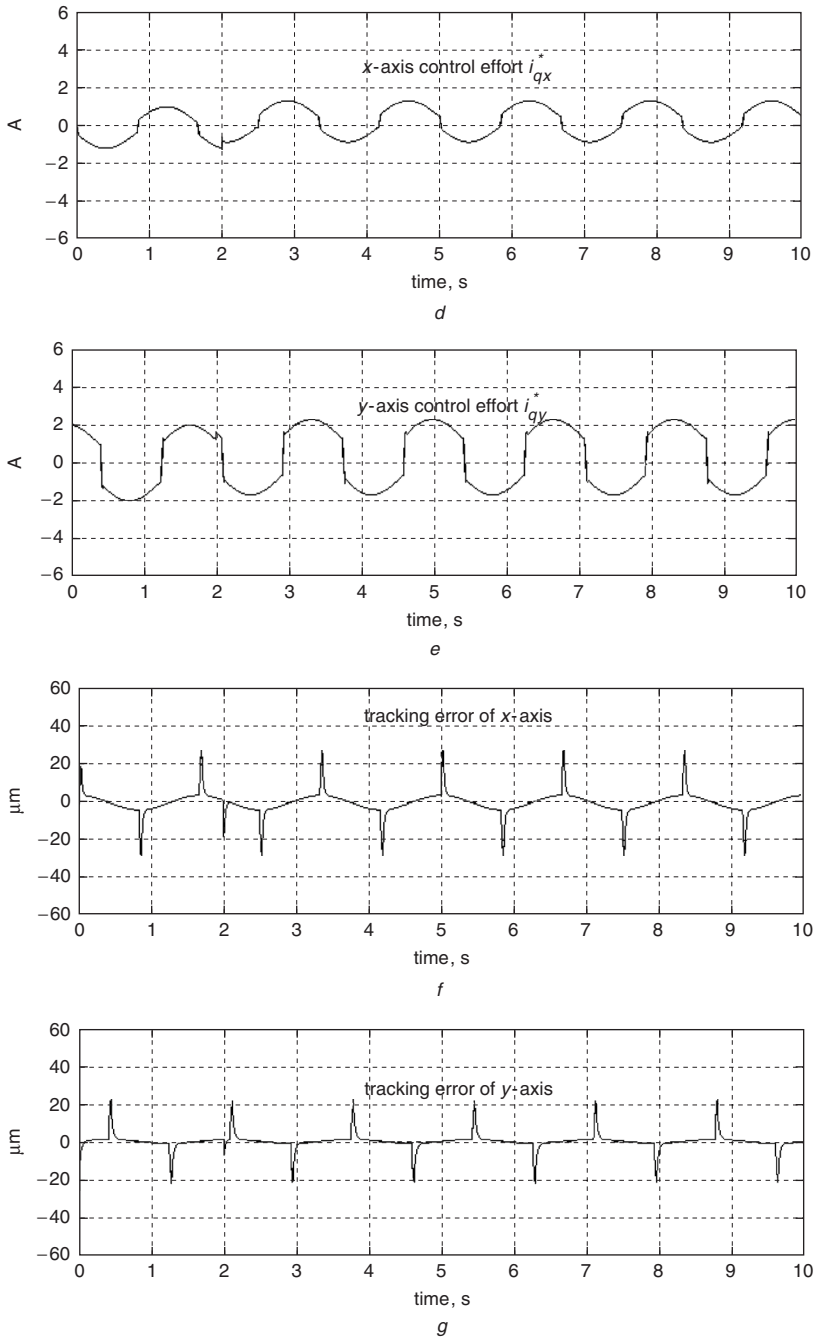


**Fig. 7** *Continued*

According to (46), an intelligent backstepping sliding-mode control law $U_T$ is proposed as follows:

$$U_T = B_n^{-1}\left[-\frac{k_1}{k_2}(z_2 - c_1 z_1) - A_n(z_2 + \dot{Y}_d - \alpha_1) - U_H - U_R + \ddot{Y}_d - \dot{\alpha}_1 - \frac{r}{k_2}\beta\right] \quad (47)$$

in which the robust controller $U_H$ is redesigned as (48) and $U_R$ is a compensated controller designed as (49).

$$U_H = \hat{H}(\boldsymbol{W}) \quad (48)$$

$$U_R = \hat{\delta} \quad (49)$$

Substituting (47), (48) and (49) into (46), the following equation can be obtained:

$$\begin{aligned}\dot{V}_3 &= z_1 z_2 - c_1 z_1^2 - r\beta^2 + k_2\beta[H - \hat{H}(\boldsymbol{W}) - \hat{\delta}] - \frac{1}{\eta_1}(\boldsymbol{W}^* - \boldsymbol{W})^T\dot{\boldsymbol{W}} - \frac{1}{\eta_2}(\delta - \hat{\delta})\dot{\hat{\delta}} \\ &= z_1 z_2 - c_1 z_1^2 - r\beta^2 + k_2\beta[H - \hat{H}(\boldsymbol{W}^*) + \hat{H}(\boldsymbol{W}^*) - \hat{H}(\boldsymbol{W})] - k_2\beta\hat{\delta} - \frac{1}{\eta_1}(\boldsymbol{W}^* - \boldsymbol{W})^T\dot{\boldsymbol{W}} - \frac{1}{\eta_2}(\delta - \hat{\delta})\dot{\hat{\delta}} \\ &= z_1 z_2 - c_1 z_1^2 - r\beta^2 + k_2\beta(\delta - \hat{\delta}) + k_2\beta(\boldsymbol{W}^* - \boldsymbol{W})^T\boldsymbol{\Gamma} - \frac{1}{\eta_1}(\boldsymbol{W}^* - \boldsymbol{W})^T\dot{\boldsymbol{W}} - \frac{1}{\eta_1}(\delta - \hat{\delta})\dot{\hat{\delta}} \end{aligned} \quad (50)$$

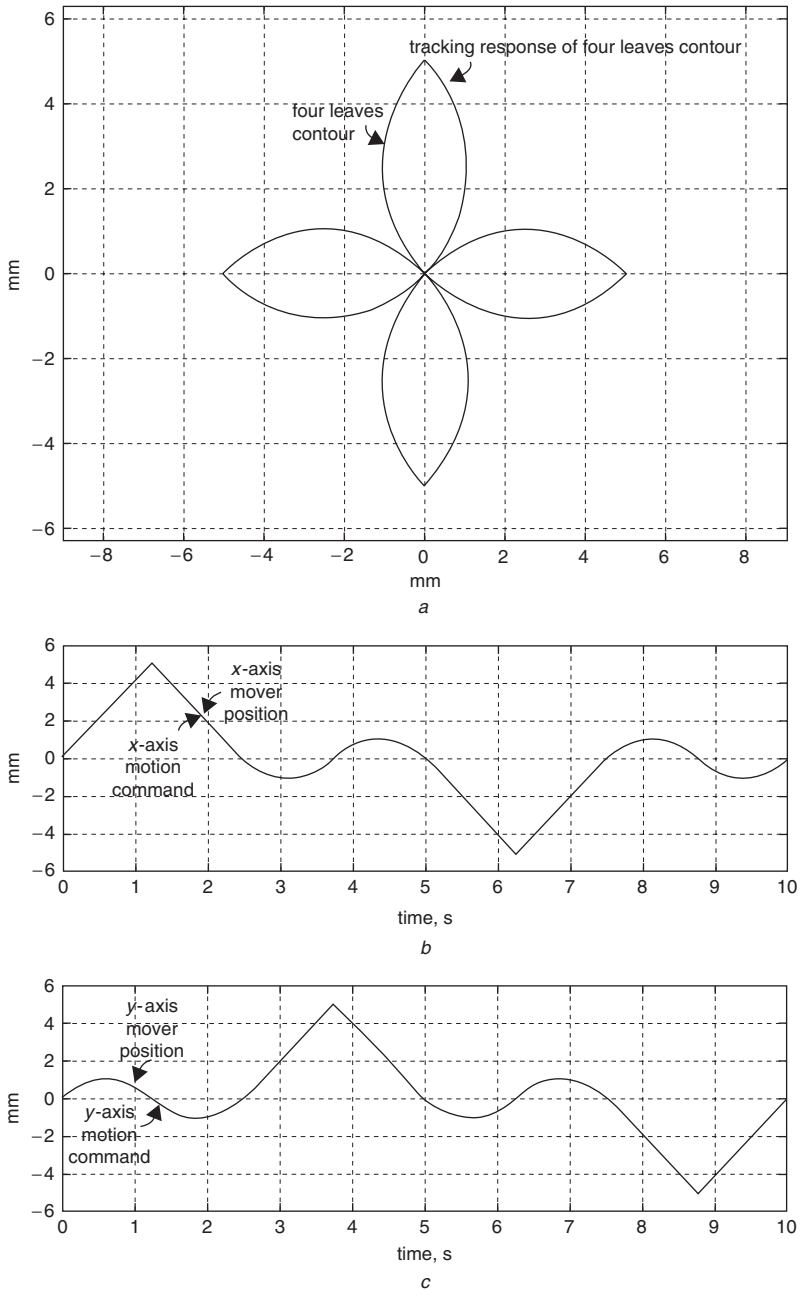


**Fig. 8** *Simulated responses of intelligent backstepping sliding-mode control system due to four leaves contour for Case 1*
*a* Tracking response of *x*–*y* table
*b* Tracking response of *x*-axis
*c* Tracking response of *y*-axis
*d* Control effort of *x*-axis
*e* Control effort of *y*-axis
*f* Tracking error of *x*-axis
*g* Tracking error of *y*-axis

If the adaptation laws for $\dot{\boldsymbol{W}}$ and $\dot{\hat{\delta}}$ are designed as follows:

$$\dot{\boldsymbol{W}} = \eta_1 k_2 \beta \boldsymbol{\Gamma} \tag{51}$$

$$\dot{\hat{\delta}} = \eta_2 k_2 \beta \tag{52}$$

Then, (50) can be rewritten as follows:

$$\dot{V}_3 = -\boldsymbol{z}^T \boldsymbol{P} \boldsymbol{z} = -\Omega(t) \leq 0 \tag{53}$$

By using Barbalat's lemma [19], it can be shown that $\Omega(t)$ tends to zero as $t \to \infty$. Therefore, $z_1$ and $z_2$ will converge to zero as $t \to \infty$. As a result, the stability of the proposed intelligent backstepping sliding-mode control system using RBFN can be guaranteed. Moreover, since the condition $\beta\dot{\beta} \leq 0$ holds, the sliding mode is guaranteed on the sliding surface $\beta = 0$. On the other hand, the guaranteed convergence of tracking error to be zero does not imply convergence of the estimated value of the lumped uncertainty to its real value. The persistent excitation condition should be satisfied for the estimated

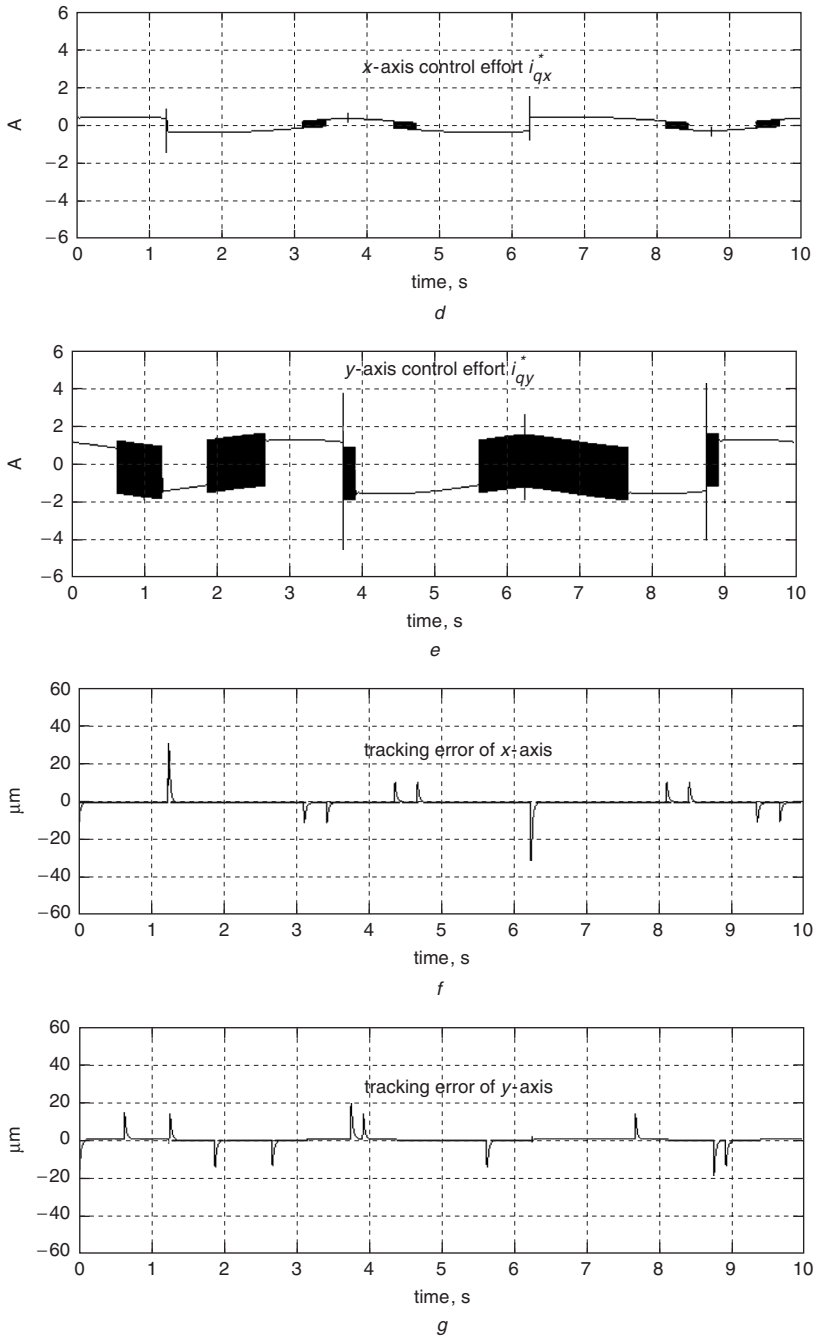


**Fig. 8** *Continued*

value to converge to its real value [19]. Using the proposed intelligent backstepping sliding-mode control design, the forward of the velocity and acceleration of the reference trajectory naturally resulted in superior tracking performance.

## 4 Simulated and experimental results

The block diagram of the DSP-based computer control two-axis motion control system is shown in Fig. 4. A TMS320C32 floating-point DSP is the core of the control computer. Moreover, the control computer includes multi-channels of analogue-to-digital converters (ADCs), digital-to-analogue converters (DACs), parallel input/output (PIO) and encoder interface. The current-controlled PWM VSI is implemented using an intelligent power module (IPM) switching component with a switching frequency of 15 kHz. Digital filters and frequency multiply by four circuits are built into the encoder interface circuits to increase the precision of position feedback. The resulting resolution is 1 μm. The field-oriented mechanism and the proposed intelligent backstepping sliding-mode control system are realised in the DSP using the 'C' and 'Assembly' language. All the programs are developed under Windows environment in the PC and are then downloaded to the EPROM. After plugging the EPROM into the DSP-based control computer, one can manipulate the computer control system via keyboard and LCD. Three-phase command currents are sent to the $x$-axis and $y$-axis motor drives using DACs. The methodology proposed for the implementation of the real-time intelligent backstepping sliding-mode control system consists of the main program, one interrupt service routine (ISR) and one subroutine 'control' in the DSP. In the main program, parameters and input/output (I/O) initialisation

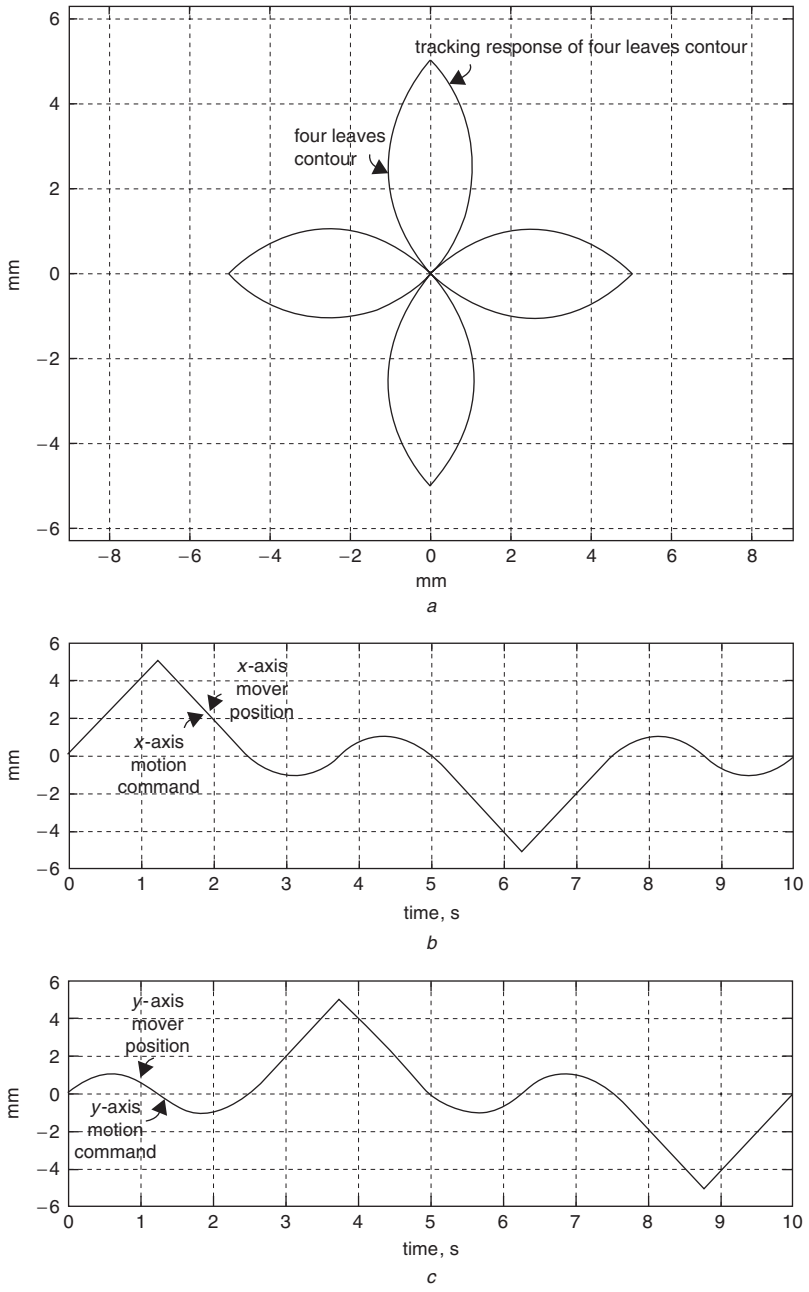


**Fig. 9** *Simulated responses of intelligent backstepping sliding-mode control system due to four leaves contour for Case 2*
*a* Tracking response of *x–y* table
*b* Tracking response of *x*-axis
*c* Tracking response of *y*-axis
*d* Control effort of *x*-axis
*e* Control effort of *y*-axis
*f* Tracking error of *x*-axis
*g* Tracking error of *y*-axis

are set first then the interrupt interval for the ISR is set. After enabling the interrupt, the ISR with 0.2 ms sampling rate is used for the encoder interface and field-oriented mechanism. The ISR reads the mover position from the linear scale and Hall sensor and gets the control effort $i_{qx}^*$, $i_{qy}^*$ from the subroutine 'control' to calculate the three-phase current commands via field-oriented mechanism, then sends the calculated three-phase current commands to the *x*-axis and *y*-axis motor drives via DACs. Since the DSP control computer has only one hardware interrupt available, a parameter $\xi$ in the ISR is used to record the executing times of the ISR. When the parameter $\xi$ is equal to 5, the subroutine 'control' begins to execute resulting in 1.0 ms sampling rate. The subroutine 'control' first reads the mover position from the encoder then calculates the motor velocity $v_x$, $v_y$ and the control effort $i_{qx}^*$, $i_{qy}^*$ according to the proposed intelligent backstepping sliding-mode control algorithm.

## 4.1 Contour planning

The contour planning is very important to control the *x–y* table effectively. The circle and four leaves contours are adopted in this study to show the control performance of the proposed intelligent backstepping sliding-mode control system. Although the contour planning is for two dimensions of motion control, in practical

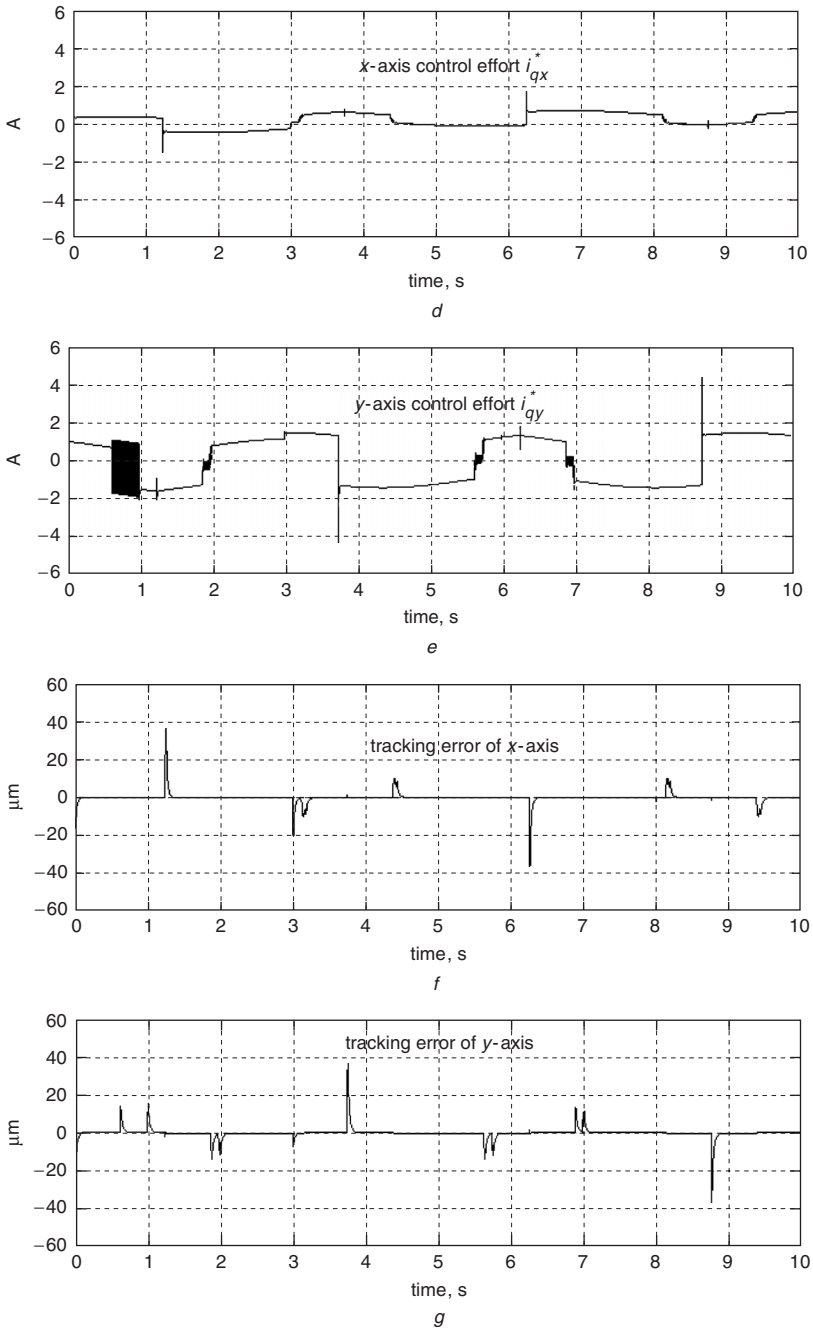


**Fig. 9** *Continued*

applications the motion commands of $x$-axis and $y$-axis are designed individually. The circle contour in Fig. 5*a* can be described as:

$$\varphi_i = \varphi_{i-1} + \Delta\varphi,\ X_i = R\cos(\varphi_i),\ Y_i = R\sin(\varphi_i) \quad (54)$$

where $\Delta\varphi$ is the variation value of the angle; $R$ is the radius of the circle; $X_i$ is the command contour of the $x$-axis; and $Y_i$ is the command contour of the $y$-axis. According to the contour function, the circle contour can be generated by the accumulation of the angle with the changing of time. Moreover, the speed of the rotor can be changed with the value of $\Delta\varphi$. The four leaves contour is shown in Fig. 5*b* in which the motion can be divided into five parts: **a**–**e**. The four leaves contour can be described as follows:

**a** trajectory: $\left(\varphi_i\colon \frac{3}{4}\pi \rightarrow \frac{1}{4}\pi\right)$, $X_i = O_{x1} + R\cos(\varphi_i)$,

$$Y_i = O_{y1} + R\sin(\varphi_i) \quad (55)$$

**b** trajectory: $\left(\varphi_i\colon -\frac{1}{4}\pi \rightarrow -\frac{5}{4}\pi\right)$, $X_i = O_{x2} + R\cos(\varphi_i)$,

$$Y_i = O_{y2} + R\sin(\varphi_i) \quad (56)$$

**Table 1: Performance measures of backstepping sliding-mode control system (simulation)**

| Tracking errors (μm) | Contours and cases | | | |
|---|---|---|---|---|
| | Circle for Case 1 | Four leaves for Case 1 | Circle for Case 2 | Four leaves for Case 2 |
| Maximum | 68.1061 | 29.1909 | 92.0715 | 51.7869 |
| Average | 54.3696 | 24.3874 | 58.1592 | 32.9867 |
| Standard deviation | 12.9987 | 7.8078 | 22.3529 | 20.3481 |

**Table 2: Performance measures of intelligent backstepping sliding-mode control system (simulation)**

| Tracking errors (μm) | Contours and cases | | | |
|---|---|---|---|---|
| | Circle for Case 1 | Four leaves for Case 1 | Circle for Case 2 | Four leaves for Case 2 |
| Maximum | 18.8847 | 31.1009 | 27.4265 | 36.8281 |
| Average | 4.4734 | 1.0687 | 4.6100 | 1.2298 |
| Standard deviation | 4.0316 | 3.0921 | 5.1419 | 3.7026 |

$$\mathbf{c}\ \text{trajectory:}\left(\varphi_i\colon \frac{1}{4}\pi \rightarrow -\frac{3}{4}\pi\right),\ X_i = O_{x3} + R\cos(\varphi_i),\quad Y_i = O_{y3} + R\sin(\varphi_i) \tag{57}$$

$$\mathbf{d}\ \text{trajectory:}\left(\varphi_i\colon \frac{3}{4}\pi \rightarrow -\frac{1}{4}\pi\right),\ X_i = O_{x4} + R\cos(\varphi_i),\quad Y_i = O_{y4} + R\sin(\varphi_i) \tag{58}$$

$$\mathbf{e}\ \text{trajectory:}\left(\varphi_i\colon -\frac{3}{4}\pi \rightarrow -\frac{5}{4}\pi\right),\ X_i = O_{x1} + R\cos(\varphi_i),\quad Y_i = O_{y1} + R\sin(\varphi_i) \tag{59}$$

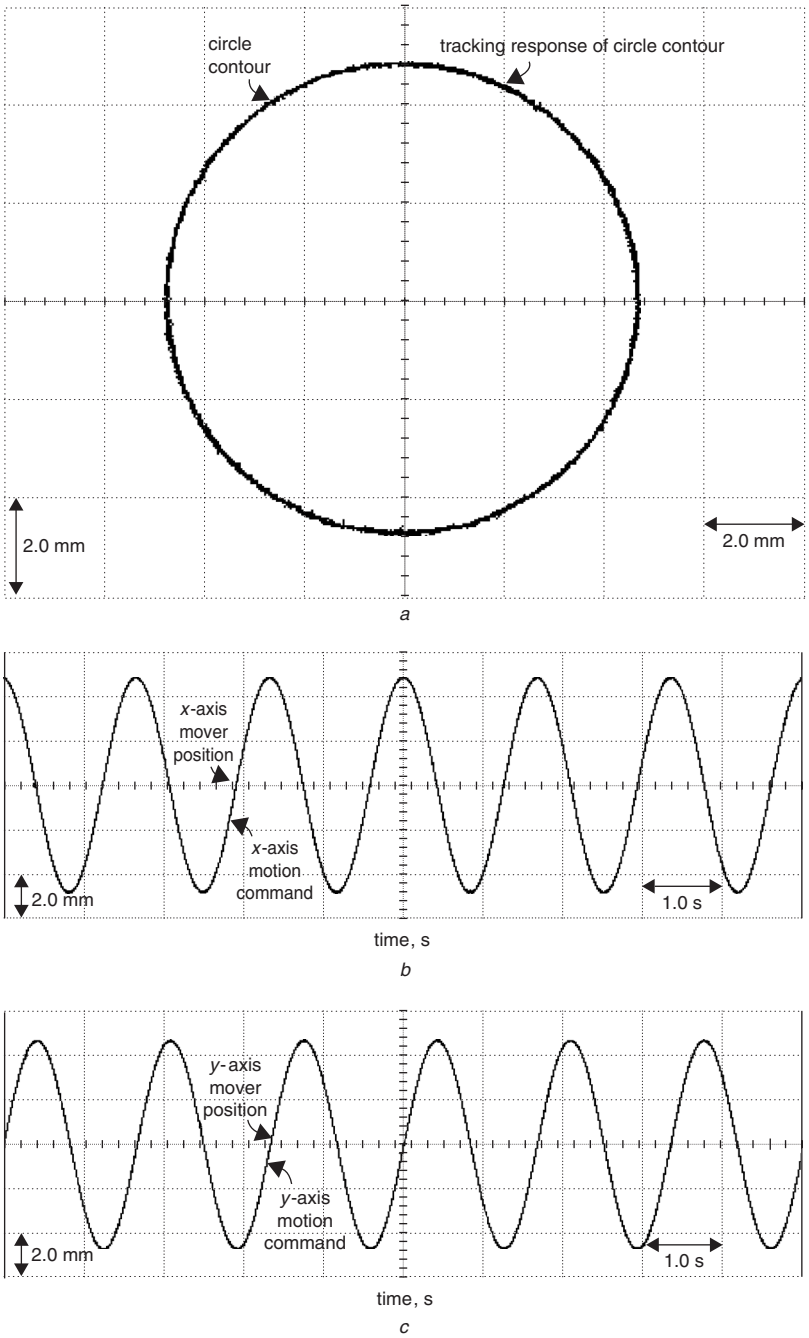


**Fig. 10** *Experimental responses of intelligent backstepping sliding-mode control system due to circle contour for nominal condition*
*a* Tracking response of *x*–*y* table
*b* Tracking response of *x*-axis
*c* Tracking response of *y*-axis
*d* Control effort of *x*-axis
*e* Control effort of *y*-axis
*f* Tracking error of *x*-axis
*g* Tracking error of *y*-axis

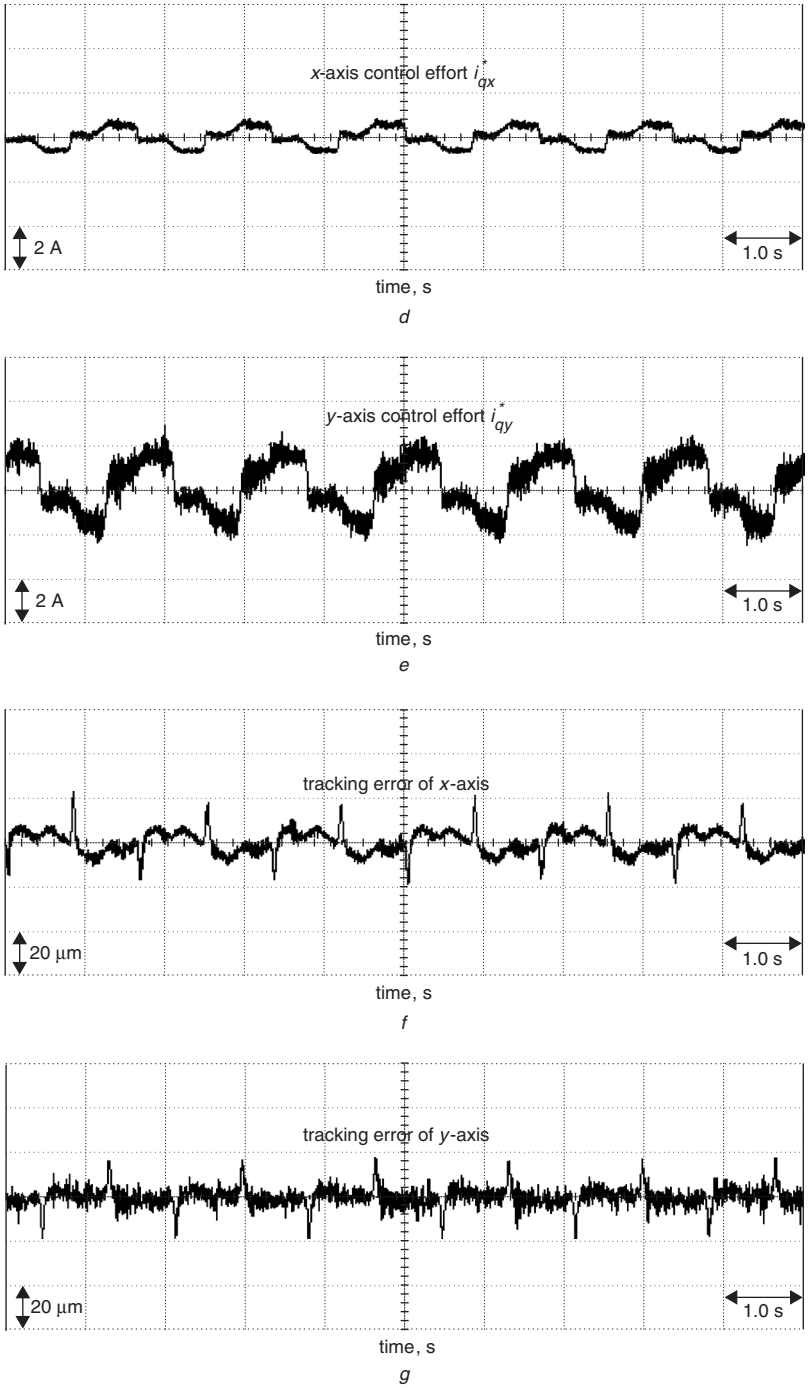


**Fig. 10** *Continued*

where $(O_{xi}, O_{yi})$ is the centre of each circle and $\varphi_i = \varphi_{i-1} + \Delta\varphi$. According to the contour function, the four leaves contour can also be generated by the accumulation of the angle with the changing of time. In addition, the tracking speed of the contour can also be changed with the value of $\Delta\varphi$.

### 4.2 Performance measures

To measure the performance of the backstepping sliding-mode control system and intelligent backstepping sliding-mode control system using RBFN, the maximum tracking error $T_M$, the average tracking error $m$ and the standard deviation of the tracking error $T_S$ for the contour tracking are defined as follows:

$$T_M = \max_k \sqrt{T_x(k)^2 + T_y(k)^2}, \quad \text{where } T_i(k) = d_{mi}(k) - d_i(k),\ i = x,\ y \tag{60}$$

$$m = \sum_{k=1}^{n} T(k)/n, \text{ where } T(k) = \sqrt{T_x(k)^2 + T_y(k)^2} \tag{61}$$

$$T_S = \sqrt{\sum_{k=1}^{n} (T(k) - m)^2/n} \tag{62}$$

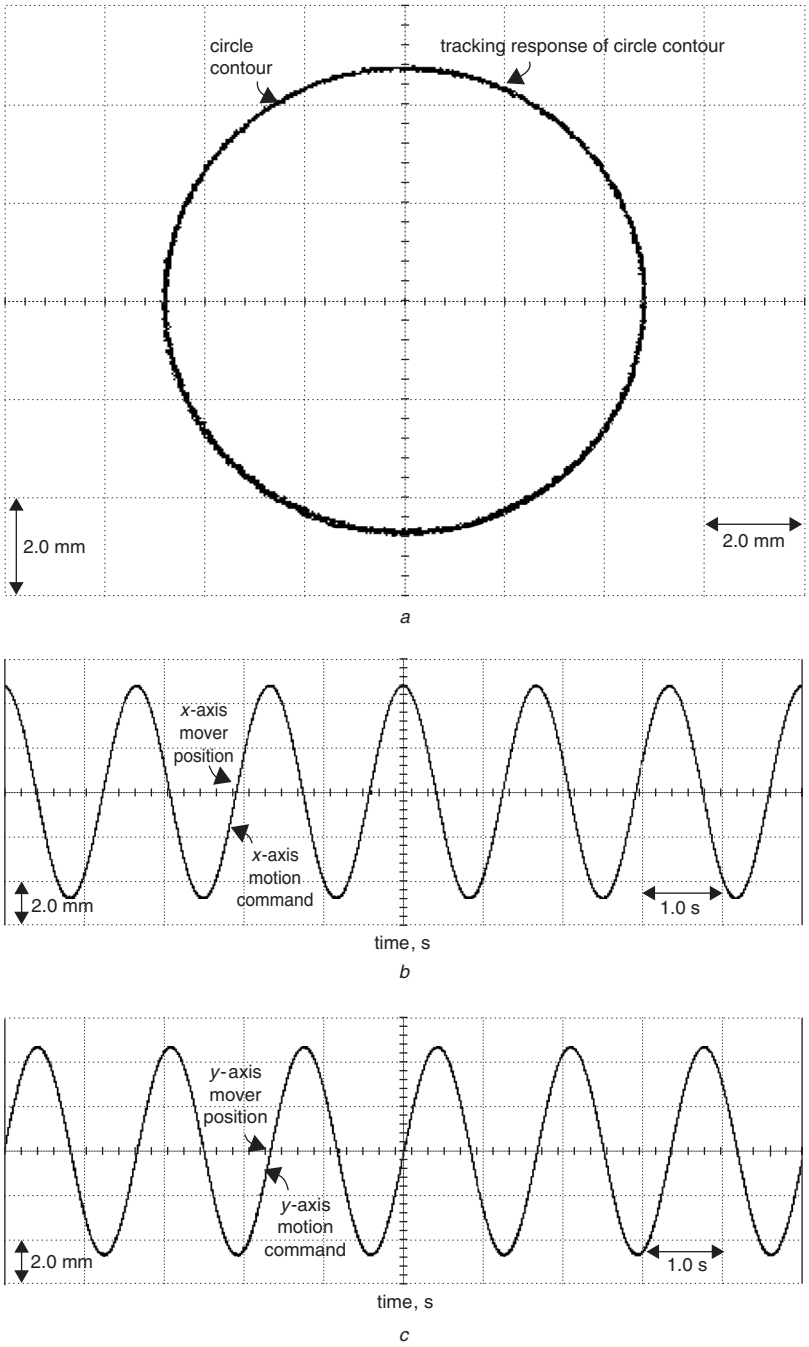


**Fig. 11** *Experimental responses of intelligent backstepping sliding-mode control system due to circle contour for parameter variation condition*
*a* Tracking response of *x*–*y* table
*b* Tracking response of *x*-axis
*c* Tracking response of *y*-axis
*d* Control effort of *x*-axis
*e* Control effort of *y*-axis
*f* Tracking error of *x*-axis
*g* Tracking error of *y*-axis

The comparison of the control performance can be easily shown using the maximum tracking error and the average tracking error. Moreover, the oscillation of the contour tracking can be measured by the standard deviation of the tracking error.

### 4.3 Simulation

To investigate the effectiveness of the proposed intelligent backstepping sliding-mode control algorithm, two simulated cases are considered in the following:

$$\text{Case 1: } M_x = \bar{M}_x, \quad M_y = \bar{M}_y \tag{63}$$

$$\text{Case 2: } M_x = 3 * \bar{M}_x,\ M_y = 3 * \bar{M}_y \text{ and } F_{Lx} = F_{Ly} = 30\,N \text{ at } 3\,\text{s} \tag{64}$$

The simulation is carried out using the 'Matlab' package. To demonstrate the control performance of the proposed control system with different contours, the simulated results

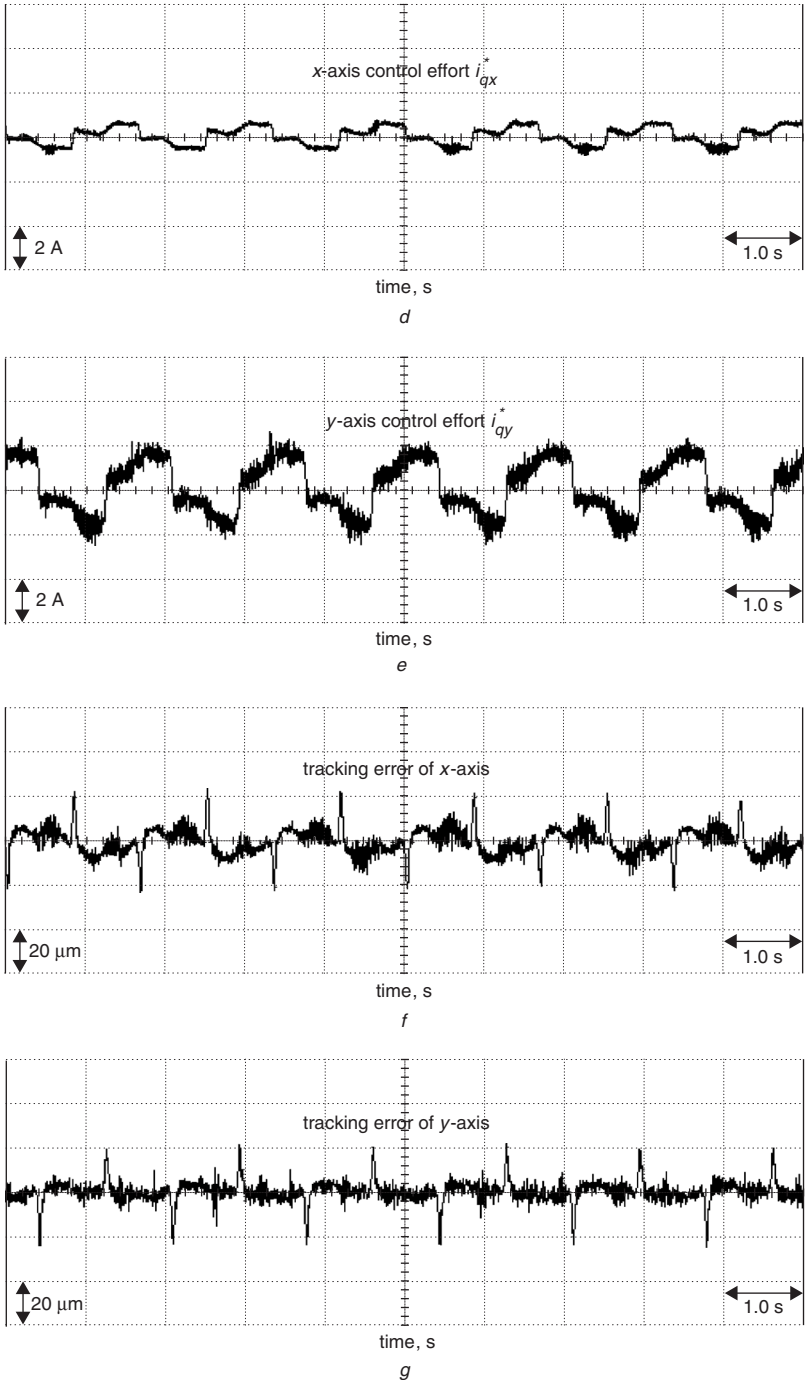


**Fig. 11** *Continued*

due to the tracking of circle and four leaves contours are given. The parameters of the intelligent backstepping sliding-mode control system are given as follows:

$$c_{1x} = 500, \quad k_{1x} = 450, \quad k_{2x} = 440,$$
$$r_x = 410, \quad \eta_{1x} = 0.015, \quad \eta_{2x} = 0.025 \tag{65}$$

$$c_{1y} = 600, \quad k_{1y} = 550, \quad k_{2y} = 540,$$
$$r_y = 510, \quad \eta_{1y} = 0.01, \quad \eta_{2y} = 0.02 \tag{66}$$

All the parameters in the proposed control systems are chosen to achieve the best transient control performance in both the simulation and experimentation considering the requirement of stability. The coefficients of the friction model used in this study are as follows:

$$F_{Cx} = 8.0, \quad F_{Sx} = 28.0, \quad v_{Sx} = 1000.24, \quad K_{vx} = 200.12 \tag{67}$$

$$F_{Cy} = 16.0, \quad F_{Sy} = 94.0, \quad v_{Sy} = 4000.24, \quad K_{vy} = 200.12 \tag{68}$$

To show the effectiveness of the intelligent backstepping sliding-mode control system with small neurons, the RBFN has two, nine and one neurons at the input, hidden and output layers, respectively. In addition, the initial values of

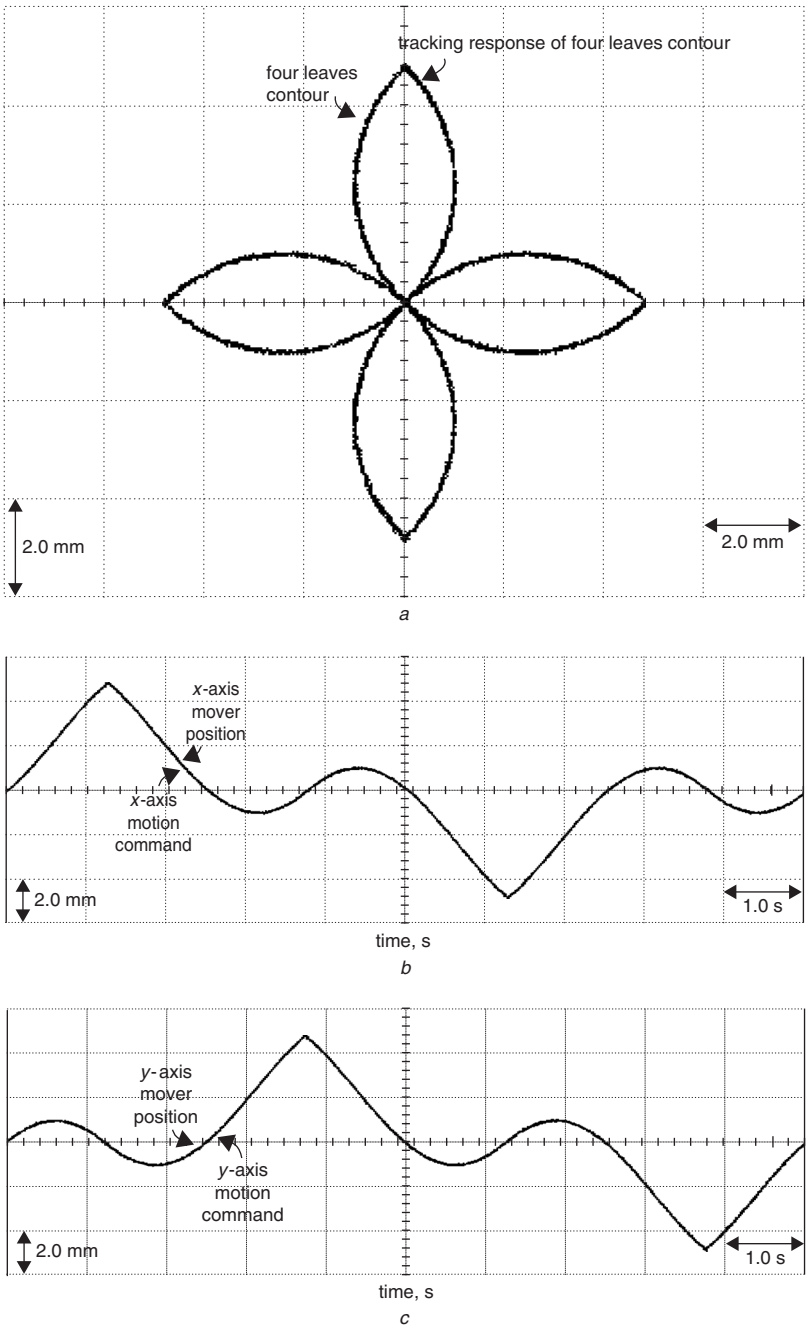


**Fig. 12** *Experimental responses of intelligent backstepping sliding-mode control system due to four leaves contour for nominal condition*
*a* Tracking response of *x–y* table
*b* Tracking response of *x*-axis
*c* Tracking response of *y*-axis
*d* Control effort of *x*-axis
*e* Control effort of *y*-axis
*f* Tracking error of *x*-axis
*g* Tracking error of *y*-axis

the connection weights are initialised to zero. The means of the Gaussian function are distributed in the range $[-1, 1]$ and all the standard deviations are 2.0.

The simulated results of the proposed intelligent backstepping sliding-mode control system shown in Fig. 2 are demonstrated as follows. The tracking responses of the *x–y* table, control efforts and tracking errors of *x*-axis and *y*-axis due to the circle contour for Case 1 and Case 2 are shown in Figs. 6 and 7, respectively. The tracking responses of the *x–y* table, control efforts and tracking errors of *x*-axis and *y*-axis due to the four leaves contour for Case 1 and Case 2 are shown in Figs. 8 and 9, respectively. From the simulated results, perfect tracking responses can be achieved for both cases. Robust control characteristics can be obtained with regard to parameter variation and external disturbance.

To show the improvement of the control performance of the proposed intelligent backstepping sliding-mode control system, the backstepping sliding-mode control system shown in (31) is adopted to control the *x–y* table for comparison of the control performance. The lumped uncertainty bounds, $\rho_x = 3.6$ and $\rho_y = 5.0$, are determined by considering the possible perturbed range of parameter variation, external disturbance, cross-coupled interference and friction force. The performance measures of the

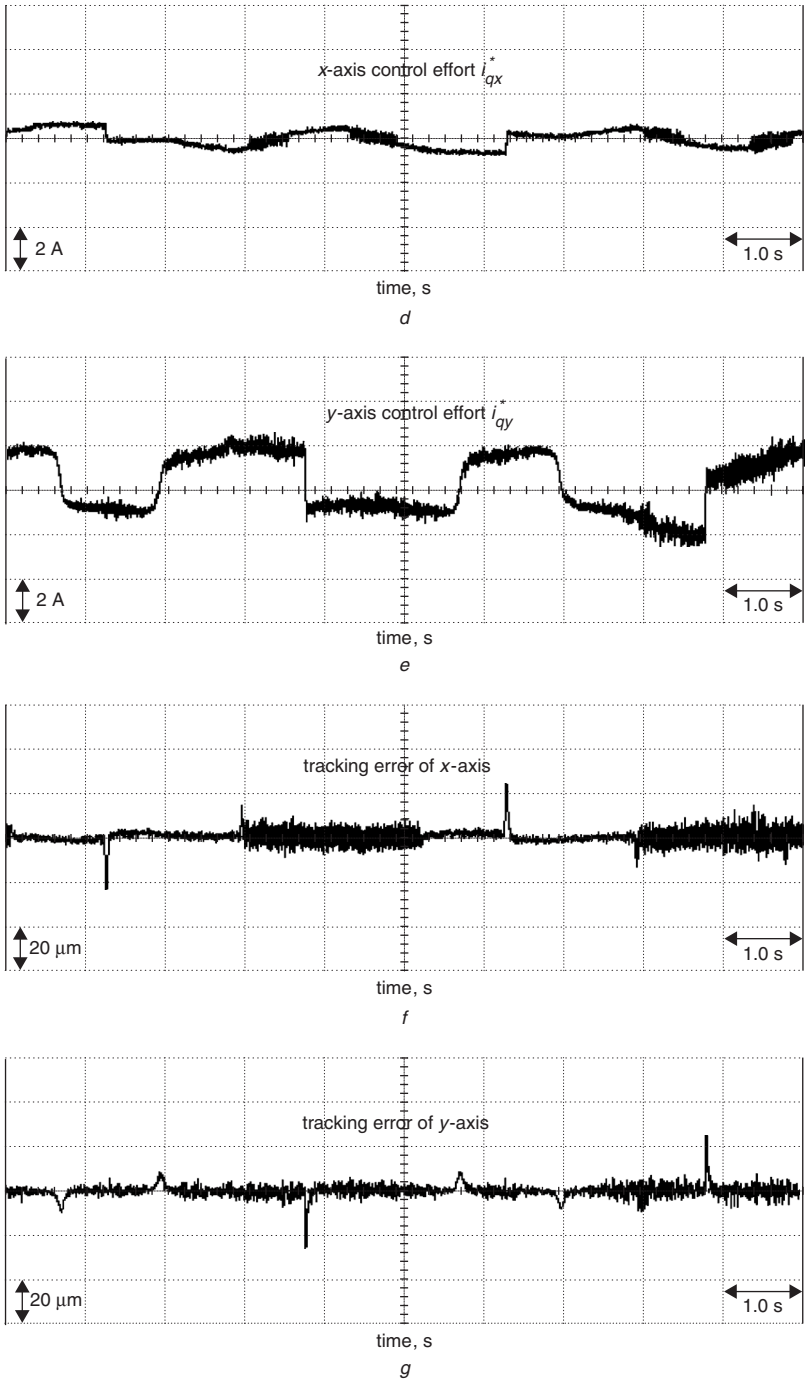


**Fig. 12** *Continued*

backstepping sliding-mode control system and intelligent backstepping sliding-mode control system using maximum tracking error, the average tracking error and standard deviation of the tracking error for the tracking of the circle and four leaves contours are shown in Tables 1 and 2, respectively. From the results shown in Table 1, although the parameters of the backstepping sliding-mode control system are chosen to be the same as the proposed intelligent backstepping sliding-mode control system, good tracking responses still cannot be obtained. Therefore, higher measures of tracking errors result. Serious measures of tracking errors due to degenerate responses result in Case 2. Comparing the performance measures of the backstepping sliding-mode control system and the proposed intelligent backstepping sliding-mode control system, the proposed control system is more suitable for implementation to control the $x$–$y$ table when uncertainties of various reference contours occur.

### 4.4 Experimentation

Two test conditions are provided in the experimentation, which are the nominal condition and the parameter variation condition. The parameter variation condition is the addition of one iron disc with a mass 20 kg on the mover of the $x$–$y$ table. The experimental results of the tracking responses of the $x$–$y$ table, the control efforts and the tracking errors of the $x$-axis and $y$-axis using the proposed intelligent backstepping sliding-mode control system due to circle and four leaves contours for the nominal condition are shown in Figs. 10 and 12. The experimental results of the tracking response of the $x$–$y$ table, the control efforts and the tracking errors of the

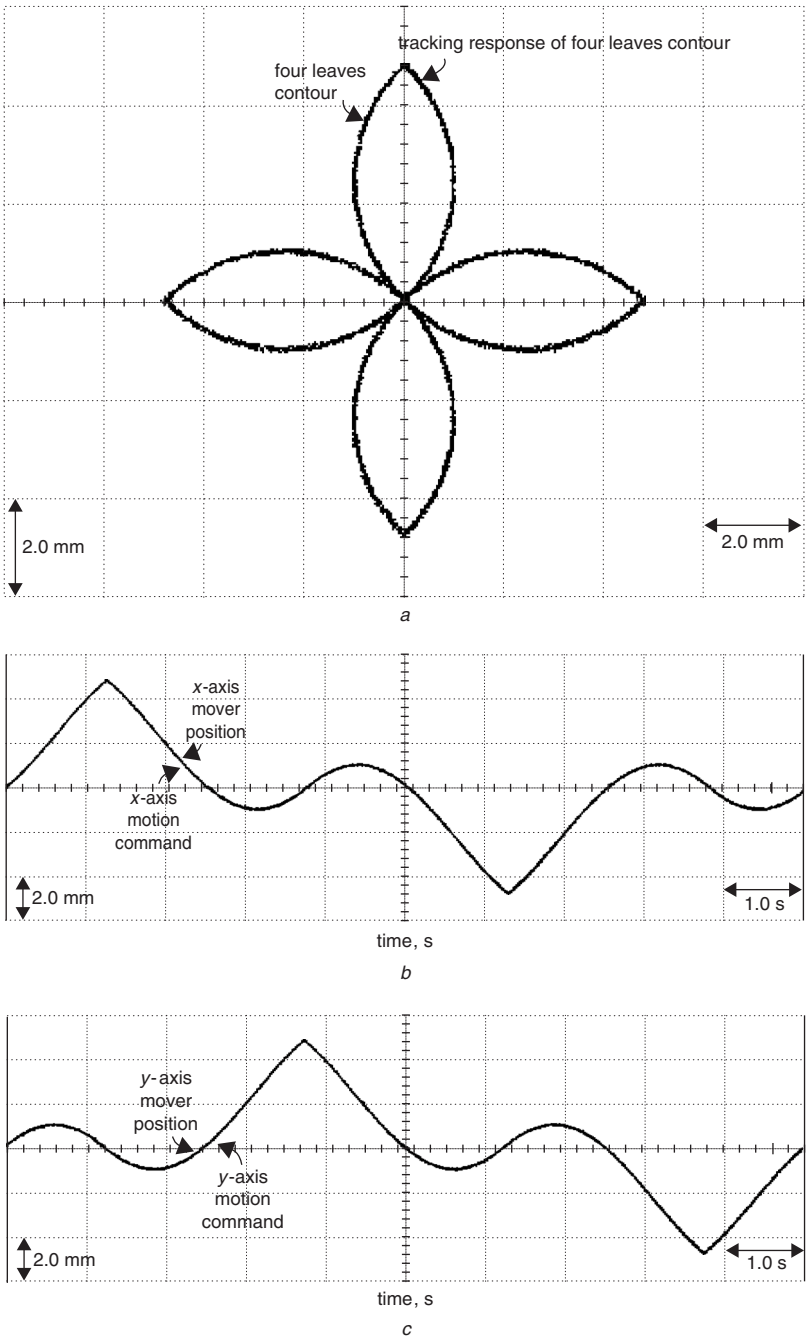


**Fig. 13** *Experimental responses of intelligent backstepping sliding-mode control system due to four leaves contour for parameter variation condition*
*a* Tracking response of *x*–*y* table
*b* Tracking response of *x*-axis
*c* Tracking response of *y*-axis
*d* Control effort of *x*-axis
*e* Control effort of *y*-axis
*f* Tracking error of *x*-axis
*g* Tracking error of *y*-axis

*x*-axis and *y*-axis using the proposed intelligent backstepping sliding-mode control system due to circle and four leaves contours for the parameter variation condition are shown in Figs. 11 and 13. From the experimental results, good tracking responses of the *x*–*y* table can be obtained at both the nominal and the parameter variation conditions. In addition, the robust control characteristics of the proposed control scheme under the occurrence of parameter variation can be clearly observed. Additionally, the resultant chattering phenomena in the control efforts as shown in Figs. 10*d*, 10*e*, 11*d*, 11*e*, 12*d*, 12*e*, 13*d* and 13*e* are due to the time-varying and nonlinear characteristics of the friction force.

To show the improvement of control performance of the proposed intelligent backstepping sliding-mode control system, the backstepping sliding-mode control system shown in (31) is also adopted in the experimentation to control the *x*–*y* table for comparison. The performance measures of the backstepping sliding-mode control system and intelligent backstepping sliding-mode control system for the circle and four leaves contours tracking at the nominal condition and the parameter variation condition

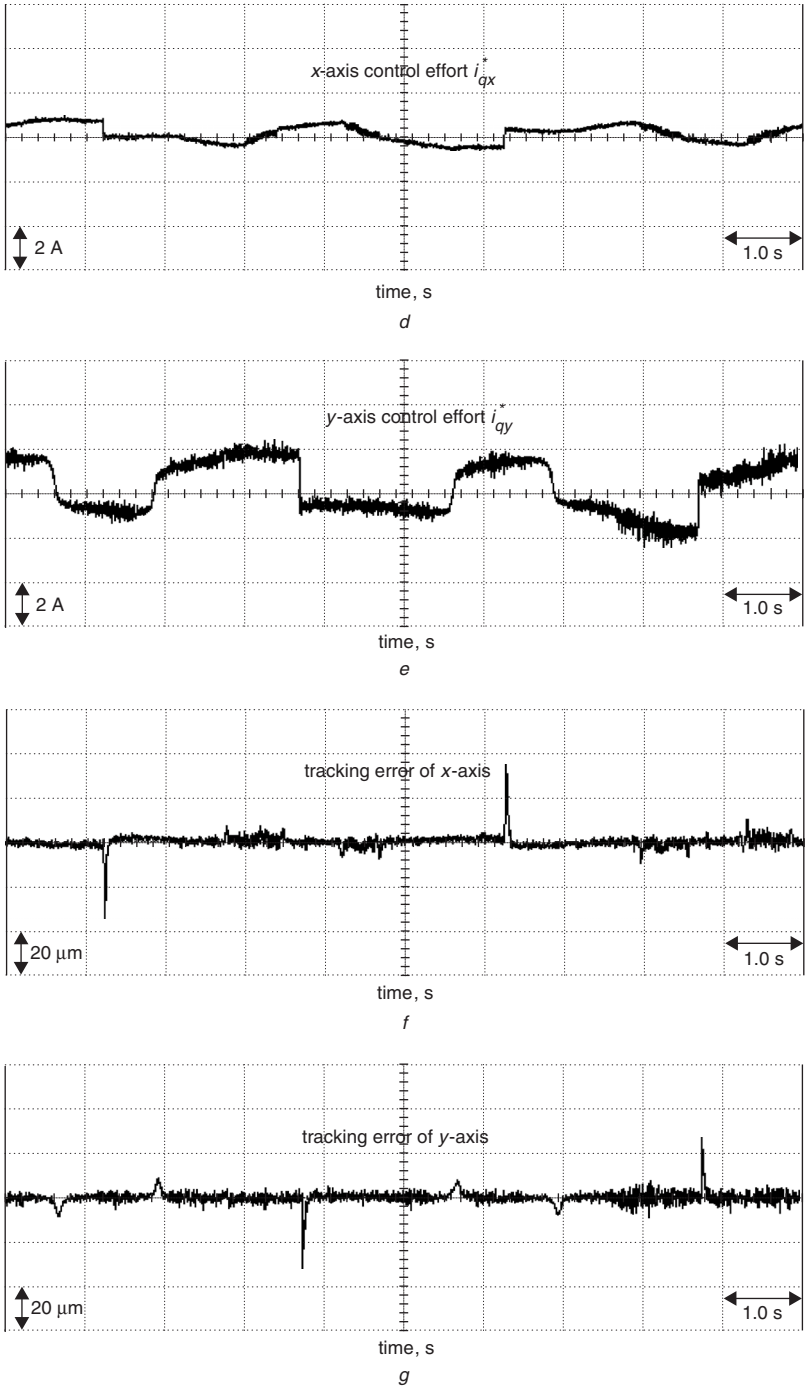


**Fig. 13** *Continued*

**Table 3: Performance measures of backstepping sliding-mode control system (experimentation)**

| Tracking errors (μm) | Contours and cases | | | |
|---|---|---|---|---|
| | Circle for nominal case | Four leaves for nominal case | Circle for parameter variation case | Four leaves for parameter variation case |
| Maximum | 50.8265 | 56.5779 | 52.6751 | 57.3275 |
| Average | 29.2322 | 31.8618 | 31.1625 | 30.6834 |
| Standard deviation | 7.6943 | 9.4196 | 8.6331 | 8.6992 |

**Table 4: Performance measures of intelligent backstepping sliding-mode control system (experimentation)**

| Tracking errors (μm) | Contours and cases | | | |
|---|---|---|---|---|
| | Circle for nominal case | Four leaves for nominal case | Circle for parameter variation case | Four leaves for parameter variation case |
| Maximum | 25.4183 | 29.4430 | 29.2761 | 36.5005 |
| Average | 6.5715 | 3.4386 | 6.5897 | 2.9953 |
| Standard deviation | 4.1196 | 3.4411 | 4.5985 | 3.2559 |

are shown in Tables 3 and 4, respectively. From the measures at nominal condition, although the parameters of the backstepping sliding-mode control system are chosen the same as the proposed intelligent backstepping sliding-mode control system, good tracking responses cannot be achieved. Therefore, higher measures of tracking errors result. Serious measures of tracking errors due to degenerated responses in the experimentation also result with regard to parameter variation for the backstepping sliding-mode control system.

## 5 Conclusions

This paper has successfully demonstrated the application of an intelligent backstepping sliding-mode control system using RBFN to control an $x$–$y$ table consisting of two field-oriented control PMLSM servo drives for reference contours. First, the principle of the field-oriented control PMLSM servo drive was introduced. Then, a robust control system was designed in the sense of backstepping control technique. To relax the requirement for the bound of lumped uncertainty, an RBFN with simple network structure was proposed to adapt the lumped uncertainty in real time. In addition, an online parameter training methodology, which is derived using the Lyapunov stability theorem, was proposed to increase the learning capability of the RBFN. The proposed intelligent backstepping sliding-mode control system using RBFN is robust for parameter variations, external disturbances, cross-coupled interference and frictional force at different trajectories. Finally, simulation and experimentation were carried out using circle and four leaves reference contours to test the effectiveness of the proposed control scheme. The major contributions of this study are: (i) the successful derivation of adaptive learning algorithms based on Lyapunov stability for an RBFN; (ii) the successful development of an intelligent backstepping sliding-mode control system using RBFN to confront the parameter variations and disturbances, including cross-coupled interference and friction force; (iii) the successful application of the intelligent backstepping sliding-mode control system using RBFN on a two-axis motion control system to track different reference contours with robust control performance.

## 6 Acknowledgment

The author would like to acknowledge the financial support of the National Science Council of Taiwan, Republic of China, through its grant NSC 93-2213-E-259-002.

## 7 References

1 Groover, M.P.: 'Fundamentals of modern manufacturing: materials, process and systems' (Prentice-Hall, Upper Saddle River, NJ, USA, 1996)
2 Kim, D.I., and Yim, C.H.: 'All digital high performance controller for spindle motor in CNC machine tool'. Proc. IEEE Int. Conf. Electric Machines and Drives, 1997, pp. 1997–1999
3 Hanafi, D., Tordon, M., and Katupitiya, J.: 'An active axis control system for a conventional CNC machine'. Proc. IEEE/ASME Int. Conf. Advanced Intelligent Mechatronics, 2003, pp. 1188–1193
4 Lim, H., Seo, J.W., and Choi, C.H.: 'Position control of XY table in CNC machining center with nonrigid ballscrew'. Proc. American Control Conf., Chicago, IL, USA, 2000, pp. 1542–1546
5 Lewis, F.L., Tim, W.K., Wang, L.Z., and Li, Z.X.: 'Deadzone compensation in motion control systems using adaptive fuzzy logic control', *IEEE Trans. Control Syst. Tech.*, 1999, **7**, (6), pp. 731–742
6 Park, E.C., Lim, H., and Choi, C.H.: 'Position control of X-Y table at velocity reversal using presliding friction characteristics', *IEEE Trans. Control Syst. Tech.*, 2003, **11**, (1), pp. 24–31
7 Boldea, I., and Nasar, S.A.: 'Linear electric actuators and generators' (Cambridge University Press, London, 1997)
8 Sanada, M., Morimoto, S., and Takeda, Y.: 'Interior permanent magnet linear synchronous motor for high-performance drives', *IEEE Trans. Ind. Appl.*, 1997, **33**, (4), pp. 966–972
9 Kempf, C.J., and Kobayashi, S.: 'Disturbance observer and feedforward design for a high-speed direct-drive positioning table', *IEEE Trans. Control Syst. Tech.*, 1999, **7**, (5), pp. 513–526
10 Lin, F.J., Lin, C.H., and Hong, C.M.: 'Robust control of linear synchronous servo drive using disturbance observer and recurrent neural network compensator', *IEE Proc. Electr. Power Appl.*, 2000, **147**, (4), pp. 263–272
11 Lin, F.J., Wai, R.J., and Hong, C.M.: 'Hybrid supervisory control using recurrent fuzzy neural network for tracking periodic input', *IEEE Trans. Neural Netw.*, 2001, **12**, (1), pp. 68–88
12 Sankaranarayanan, S., and Khorrami, F.: 'Adaptive variable structure control and application to friction compensation'. IEEE CDC Conf. Rec., 1997, pp. 4159–4164
13 Maulana, A.P., Ohmori, H., and Sano, A.: 'Friction compensation strategy via smooth adaptive dynamic surface control'. IEEE CCA Conf. Rec., 1999, pp. 1090–1095
14 Kanellakopoulos, I., Kokotovic, P.V., and Morse, A.S.: 'Systematic design of adaptive controller for feedback linearizable systems', *IEEE Trans. Autom. Control*, 1991, **36**, (11), pp. 1241–1253
15 Krstic, M., Kanellakopoulos, I., and Kokotovic, P.V.: 'Nonlinear and adaptive control design' (Wiley, New York, USA, 1995)
16 Taylor, D.G.: 'Nonlinear control of electric machines: An overview', *IEEE Control Syst. Mag.*, 1994, **14**, pp. 41–51
17 Shieh, H.J., and Shyu, K.K.: 'Nonlinear sliding-mode torque control with adaptive backstepping approach for induction motor drive', *IEEE Trans. Ind. Electron.*, 1999, **46**, (2), pp. 380–389
18 Lin, F.J., and Lee, C.C.: 'Adaptive backstepping control for linear induction motor drive to track periodic references', *IEE Proc., Electr. Power Appl.*, 2000, **147**, (6), pp. 449–458
19 Slotine, J.J.E., and Li, W.: 'Applied nonlinear control' (Prentice-Hall, New Jersey, USA, 1991)
20 Stotsky, A., Hedrick, J.K., and Yip, P.P.: 'The use of sliding modes to simplify the backstepping control method'. Proc. of American Control Conf., 1997, pp. 1703–1708
21 Rios-Bolivar, M., and Zinober, A.S.I.: 'Dynamical adaptive sliding mode control of observable minimum-phase uncertain nonlinear systems' in 'Variable structure systems, sliding mode and nonlinear control' (Springer-Verlag, London, UK, 1999), pp. 211–235
22 Bartolini, G., Ferrara, A., Giacomini, L., and Usai, E.: 'Peoperties of a combined adaptive/second-order sliding mode control algorithm for some classes of uncertain nonlinear systems', *IEEE Trans. Autom. Control*, 2000, **45**, (7), pp. 1334–1341
23 Lin, F.J., Shen, P.H., and Hsu, S.P.: 'Adaptive backstepping sliding mode control for linear induction motor drive', *IEE Proc., Electr. Power Appl.*, 2002, **149**, (3), pp. 184–194
24 Jang, J.S.R., Sun, C.T., and Mizutani, E.: 'Neuro-fuzzy and soft computing: A computational approach to learning and machine intelligence' (Prentice-Hall, Upper Saddle River, NJ, USA, 1997)
25 Jang, J.S.R., and Sun, C.T.: 'Functional equivalence between radial basis function networks and fuzzy inference systems', *IEEE Trans. Neural Netw.*, 1993, **4**, pp. 156–159
26 Patino, H.D., and Liu, D.: 'Neural network-based model reference adaptive control system', *IEEE Trans. Syst. Man Cybern. B*, 2000, **30**, pp. 198–204
27 Seshagiri, S., and Khail, H.K.: 'Output feedback control of nonlinear systems using RBF neural networks', *IEEE Trans. Neural Netw.*, 2000, **11**, pp. 69–79